Global Change Biology

Global Change Biology (2013), doi: 10.1111/gcb.12283

Large-scale variations in the vegetation growing season and annual cycle of atmospheric CO_2 at high northern latitudes from 1950 to 2011

JONATHAN BARICHIVICH*, KEITH R. BRIFFA*, RANGA B. MYNENI†, TIMOTHY J. OSBORN*, THOMAS M. MELVIN*, PHILIPPE CIAIS‡, SHILONG PIAO§¶ and COMPTON TUCKER||

*Climatic Research Unit, School of Environmental Sciences, University of East Anglia, Norwich, NR4 7TJ, UK, †Department of Earth and Environment, Boston University, Boston, MA, USA, ‡Laboratory for Climate Sciences and the Environment (LSCE), Joint Unit of CEA-CNRS, Gif-sur-Yvette, France, §College of Urban and Environmental Sciences, Peking University, Beijing, China, ¶Key Laboratory of Alpine and Biodiversity, Institute of Tibetan Plateau Research, Chinese Academy of Sciences, Beijing 100085, China, ||Biospheric Sciences Branch, NASA Goddard Space Flight Center, Greenbelt, MD 20771, USA

Abstract

We combine satellite and ground observations during 1950–2011 to study the long-term links between multiple climate (air temperature and cryospheric dynamics) and vegetation (greenness and atmospheric CO_2 concentrations) indicators of the growing season of northern ecosystems (>45°N) and their connection with the carbon cycle. During the last three decades, the thermal potential growing season has lengthened by about 10.5 days ($P < 0.01$, 1982–2011), which is unprecedented in the context of the past 60 years. The overall lengthening has been stronger and more significant in Eurasia (12.6 days, $P < 0.01$) than North America (6.2 days, $P > 0.05$). The photosynthetic growing season has closely tracked the pace of warming and extension of the potential growing season in spring, but not in autumn when factors such as light and moisture limitation may constrain photosynthesis. The autumnal extension of the photosynthetic growing season since 1982 appears to be about half that of the thermal potential growing season, yielding a smaller lengthening of the photosynthetic growing season (6.7 days at the circumpolar scale, $P < 0.01$). Nevertheless, when integrated over the growing season, photosynthetic activity has closely followed the interannual variations and warming trend in cumulative growing season temperatures. This lengthening and intensification of the photosynthetic growing season, manifested principally over Eurasia rather than North America, is associated with a long-term increase (22.2% since 1972, $P < 0.01$) in the amplitude of the CO_2 annual cycle at northern latitudes. The springtime extension of the photosynthetic and potential growing seasons has apparently stimulated earlier and stronger net CO_2 uptake by northern ecosystems, while the autumnal extension is associated with an earlier net release of CO_2 to the atmosphere. These contrasting responses may be critical in determining the impact of continued warming on northern terrestrial ecosystems and the carbon cycle.

Keywords: carbon cycle, climate change, NDVI, phenology, vegetation greening

Received 29 October 2012 and accepted 25 May 2013

Introduction

The seasonal photosynthetic dynamics of northern vegetation are tightly coupled to the timing and duration of the warm season and associated snow-free and non-frozen ground conditions (Goulden *et al*., 1998; Nemani *et al*., 2003). The instrumental temperature record shows convincingly that northern terrestrial ecosystems have experienced the largest warming rates on the globe during recent decades, particularly in winter and spring (Trenberth *et al*., 2007). Warming has shifted the timing of the seasonal warmth earlier in spring and later in autumn (Burrows *et al*., 2011; Barichivich *et al*., 2012), reducing snow-cover duration and extending the length of the vegetation growing season (Keeling *et al*., 1996; Myneni *et al*., 1997). In these regions, phenology controls the seasonal onset and ending of the carbon uptake period, thereby directly affecting net ecosystem carbon balance (Goulden *et al*., 1998; Barr *et al*., 2009; Richardson *et al*., 2010) and the exchange of water and energy with the atmosphere (Peñuelas *et al*., 2009).

Earlier and longer growing seasons are generally associated with increased ecosystem carbon sequestration because more days are available for carbon uptake and biomass growth (Richardson *et al*., 2010). In some instances, however, earlier spring growth advances soil water depletion, which counteracts higher early spring

Correspondence: Jonathan Barichivich, tel. +44 (0)1603 592318, fax +44 (0) 1603 591327, e-mail: j.barichivich@uea.ac.uk

carbon assimilation through the enhancement of mid-summer drought conditions (White & Nemani, 2003; Angert *et al.*, 2005; Ciais *et al.*, 2005; Hu *et al.*, 2010). While the extension of the growing season in autumn prolongs photosynthesis in some vegetation types despite decreasing radiation levels, the net impact on seasonal ecosystem carbon balance is not always positive as soil respiration tends to increase more than photosynthesis (Piao *et al.*, 2008).

The warming-driven lengthening of the vegetation growing season by about 7–12 days during the 1980s and 1990s has produced a strong seasonal advance and increase in terrestrial photosynthetic activity at northern latitudes (Myneni *et al.*, 1997; Zhou *et al.*, 2001). This has led to a substantial phase advance and magnification of the peak-to-trough amplitude of the atmospheric CO_2 annual cycle during this period (Keeling *et al.*, 1996). Together, these observations provide evidence for a significant influence of large-scale vegetation phenology on the terrestrial carbon sink that has also been found in modeling studies (Randerson *et al.*, 1999; Lucht *et al.*, 2002; Piao *et al.*, 2007).

Large-scale variations in the duration and intensity of the vegetation growing season across the extratropical Northern Hemisphere have been widely studied using a range of approaches (Linderholm, 2006; Cleland *et al.*, 2007), but estimates are typically restricted to the satellite period over the last three decades. Most assessments of long-term changes in the seasonal photosynthetic dynamics at these large spatial scales have relied on the satellite record of Normalized Difference Vegetation Index (NDVI) derived from Advanced Very High Resolution Radiometer (AVHRR) observations from 1981 to the present (e.g., James & Kalluri, 1994; Los *et al.*, 1994; Tucker *et al.*, 2005). Since the study by Myneni *et al.* (1997), the continuous analysis of this satellite record has shown an evolving picture of progressively earlier, longer, and more productive growing seasons during recent decades throughout most of the northern-vegetated lands (e.g., Tucker *et al.*, 2001; Zhou *et al.*, 2001; Dye & Tucker, 2003; Nemani *et al.*, 2003; Piao *et al.*, 2006; Julien & Sobrino, 2009; White *et al.*, 2009; Bhatt *et al.*, 2010; Jeong *et al.*, 2011). Independent studies based on satellite observations of snow-cover (Dye & Tucker, 2003; Grippa *et al.*, 2005) and freeze-thaw dynamics extending back to 1979 (Kimball *et al.*, 2004; Smith *et al.*, 2004; Zhang *et al.*, 2011; Kim *et al.*, 2012) have confirmed the general advance and extension of the vegetation growing season at northern latitudes.

The satellite-observed changes in the duration and intensity of the vegetation growing season are broadly consistent with ground-based observational networks of local phenological and surface air temperature records (e.g., Jones & Briffa, 1995; Menzel *et al.*, 2003, 2006; Parmesan & Yohe, 2003; Schwartz *et al.*, 2006), atmospheric CO_2 concentrations (Keeling *et al.*, 1996; Piao *et al.*, 2008), and spatially continuous gridded fields of daily surface air temperatures (Christidis *et al.*, 2007; Barichivich *et al.*, 2012) extending back to the mid-20th century. However, only limited analyses of multiple long-term climate and vegetation variables exist at continental or hemispheric scales for evidence of cogent and coherent trends in vegetation activity (e.g., Dye & Tucker, 2003; Bunn *et al.*, 2005; White *et al.*, 2009; Wu *et al.*, 2012). Studies comparing changes in vegetation and climate seasonality at these large spatial scales are needed to assess the extent to which vegetation and terrestrial ecosystems are tracking the pace of the rapid climatic warming and concomitant changes in seasonality (Burrows *et al.*, 2011), particularly in spring and autumn. The relative responses of vegetation and ecosystem phenology in these shoulder seasons have significant, and often opposite, impacts on the carbon cycle (Piao *et al.*, 2008).

In this study, we combine independent streams of satellite and ground observations of NDVI, surface air temperature, snow-cover, freeze-thaw dynamics, and atmospheric CO_2 concentration covering different periods between 1950 and 2011 to conduct an integrated assessment of long-term continental and circumpolar changes in the vegetation growing season and evaluate their impact on the net carbon uptake by terrestrial ecosystems north of 45°N. Our specific aims are (i) to assess interannual and longer term temporal variations in the timing, length, and intensity of the NDVI-based photosynthetic growing season in the context of the climatically defined potential vegetation growing season, and (ii) to examine the influence of these variations on the annual cycle of atmospheric CO_2 concentration at high northern latitudes. This combined assessment of multiple interrelated variables of the climate system contributes to reduce observational uncertainties on the magnitude of the responses of terrestrial ecosystems to the rapid climate change ongoing at northern latitudes. Furthermore, it provides a robust observational benchmark for validating the large-scale variability and trends in the growing season simulated by ecosystem models.

Materials and methods

Photosynthetic growing season

We use the latest version of the biweekly 8 km NDVI data set (NDVI3g) produced from AVHRR level 1b observations by the Global Inventory Modeling and Mapping Studies (GIMMS) group at NASA Goddard Space Flight Center to characterize the photosynthetic growing season of the vegetated

land north of 45°N from 1982 to 2011 (see Table 1). This new, third generation GIMMS NDVI(3g) data set extends the record from December 2006 in the previous GIMMS NDVIg data set (Tucker *et al*., 2005) to December 2011. Like GIMMS NDVIg, it has been processed to account for orbital drift, sensor degradation, cloud cover, and aerosols. Some important issues affecting the GIMMS NDVIg dataset at northern latitudes have been corrected, such as a calibration-related lack of data north of 72°N that was rectified in GIMMS NDVI3g using SeaWiFS (Sea-viewing Wide Field-of-view sensor) instead of SPOT (Système Probatoire d'Observation de la Terre) Vegetation NDVI data for cross-sensor intercalibration (i.e., SPOT Vegetation data end at 72°N while SeaWiFS data do not). The use of SeaWiFS data for cross-calibration with the NDVI3g data also resulted in improved calibration of the data from NOAA-16, -17, and -18 due to the bilinear gains in the AVHRR instruments' channel one on these satellites. These improvements were evident by a higher correlation and closer correspondence of the NDVI3g data with Moderate Resolution Imaging Spectroradiometer (MODIS) Aqua and Terra NDVI coincident data. These and other methodological refinements, such as an improved coastal land-water mask and pixel quality flags, have considerably improved data quality for northern-vegetated lands, making NDVI3g better suited to studies of northern ecosystems as well as elsewhere. The methodology used to develop and validate the dataset has yet to be published (J.E. Pinzon, E.W. Park, C.J. Tucker, in preparation). However, the data set has already been used in several studies analyzing vegetation dynamics in northern ecosystems (e.g., Bhatt *et al*., 2010; Epstein *et al*., 2012; Fensholt & Proud, 2012; Raynolds *et al*., 2012; Xu *et al*., 2013). It has been shown that the dataset compares well with NDVI from MODIS sensors since the early 2000s (Fensholt & Proud, 2012).

Prior data processing, the Collection 5 MODIS land cover product (MCD12C1) with International Geosphere Biosphere Programme (IGBP) classes for the year 2007 (Friedl *et al*., 2010), was used to exclude from analysis grid points corresponding to croplands, cropland/natural vegetation mosaics,

Table 1 Summary of parameters used in this study to characterize the growing season and the annual cycle of atmospheric CO_2 at northern latitudes. See text for a detailed definition and description of the datasets used to derive each parameter

Parameter	Resolution	Period	Short definition
Start of season			
STH – Spring thaw	0.25° × 0.25°	1988–2007	First day of a 15-day running window with at least 12 non-frozen days between January and June
SMT – Spring snow melt	190 × 190 km	1972–2011	First week of continuous run of at least 5 snow-free weeks between January and June
STS – Start of thermal growing season	2.75° × 3.75°	1950–2011	Day when temperature rises to 5 °C in spring
SOS – Start of photosynthetic growing season	8 × 8 km	1982–2011	Day when NDVI reaches a local threshold for maximum green-up rate
End of season			
AFZ – Autumn Freeze	0.25° × 0.25°	1988–2007	First day of a 15-day running window with at least 12 days with frozen status between September and December
ETS – End of thermal growing season	2.75° × 3.75°	1950–2011	Day when temperature decreases to 5°C in autumn
EOS – End of photosynthetic growing season	8 × 8 km	1982–2011	Day when NDVI decreases to a local threshold for maximum browning rate
Length of season			
LNF – Length of non-frozen period	0.25° × 0.25°	1988–2007	Days between STH and AFZ
LTS – Length of thermal growing season	2.75° × 3.75°	1950–2011	Days between STS and ETS
LOS – Length of photosynthetic growing season	8 × 8 km	1982–2011	Days between SOS and EOS
Intensity of season			
TI-NDVI – Time integrated NDVI	8 × 8 km	1982–2011	Sum of smoothed daily-interpolated NDVI from SOS to EOS
TI-TEM – Time integrated temperature	2.75° × 3.75°	1950–2011	Sum of smoothed daily temperature from STS to ETS
CO_2 annual cycle			
SZC – Spring zero-crossing	station	1972–2010	Day when the detrended CO_2 annual cycle exceeds 0 ppm in spring
AZC – Autumn zero-crossing	station	1972–2010	Day when the detrended CO_2 annual cycle falls below 0 ppm in autumn
AMP – Amplitude CO_2 annual cycle	station	1972–2010	Annual Maximum minus annual minimum detrended seasonal CO_2 concentration

urban and built-up, and barren or sparsely vegetated land cover classes. Here, the land cover product at 0.05° resolution was spatially resampled to match the resolution of the NDVI3g dataset (1/12°) using the nearest neighbor algorithm. Then, the TIMESAT (version 3.1.1) software for time-series analysis of satellite data (Jönsson & Eklundh, 2004) was used to smooth the bi-weekly NDVI time series at each grid point with a double logistic fit to describe the yearly trajectory of the NDVI and reduce high-frequency noise. The curve-fitting procedure included adaptation to the upper envelope of the NDVI time series to minimize the influence of factors not related to vegetation dynamics, such as snow and cloud cover that generally decrease the NDVI values (Reed *et al.*, 1994; Stöckli & Vidale, 2004). We chose a double logistic function for data smoothing because it has been shown to perform better than the other approaches for modeling NDVI data from the high latitudes (Beck *et al.*, 2006; Gao *et al.*, 2008).

After smoothing, the biweekly NDVI data were linearly interpolated to daily resolution. Then, for each grid point the NDVI values corresponding to the inflection points for the maximum rate of green-up and senescence were determined from the first derivative of the long-term mean seasonal curve of smoothed NDVI data (i.e., 30-year NDVI climatology) interpolated to daily resolution. These NDVI thresholds were then used to compute the day of year for the start (SOS) and end (EOS) of the photosynthetic growing season for each year and grid box (Table 1). The length of the photosynthetic growing season (LOS) was estimated as the difference between EOS and SOS. The (greenness) 'intensity' of the photosynthetic growing season, defined here as the time-integrated NDVI (TI-NDVI) over the growing season, was computed by summing daily-interpolated smoothed NDVI values from SOS to EOS.

The threshold approach based on the local rate of change in NDVI has a better biophysical basis than using an arbitrary NDVI threshold value to estimate SOS and EOS across a wide range of vegetation types (Piao *et al.*, 2006; Jeong *et al.*, 2011; Tan *et al.*, 2011). We also examined two other threshold-based approaches for estimating the start, end, and length of the photosynthetic growing season from the smoothed NDVI data. One was based on the NDVI thresholds corresponding to the beginning of the green-up and senescence periods estimated from the second derivative of the NDVI climatology. The other used an arbitrary threshold of 25% of the yearly amplitude of the annual cycle of NDVI. We found that the three methods produce very similar results (Fig. S1), but we chose the approach based on the first derivative for consistency with earlier studies and because of its better biophysical basis (e.g., Piao *et al.*, 2006; Jeong *et al.*, 2011), though we note that it has a slightly higher correlation with the climatically defined potential growing season.

It has been shown that northern latitude phenological patterns retrieved from AVHRR GIMMS NDVI data can differ significantly from other satellite sensors (Zhang *et al.*, 2013). To assess the sensitivity of our results to dataset version and satellite sensor we also computed the suite of phenological parameters using the previous 15-day GIMMS NDVIg data set over the period 1982–2006 (available at http://glcf.umd.edu/data/gimms/) and 16-day Terra MODIS NDVI from the MOD13C1 product (0.05°) during the overlapping period 2001–2011 (available at http://lpdaac.usgs.gov/products/modis). Terra MODIS NDVI data are of higher radiometric and geometric quality than AVHRR data and have been atmospherically corrected and masked for water, clouds, and shadows. The data sets were first remapped to match the 1/12° GIMMS NDVI3g grid using bilinear interpolation and then processed following the same procedure used for GIMMS NDVI3g.

Potential growing season: thermal and non-frozen seasons

Low temperatures and frozen ground conditions strongly limit the metabolic activity of northern vegetation (Jarvis & Linder, 2000; Nemani *et al.*, 2003). We therefore conceptually define the potential vegetation growing season as that period of the year when air temperatures remain above a certain threshold that allows vegetation growth (thermal growing season) or alternatively when the ground surface is not frozen (non-frozen season).

We used gridded daily mean air temperatures from the HadGHCND data set to characterize the thermal growing season for northern vegetation from 1950 to 2011 on a regular 2.75° × 3.75° grid (Caesar *et al.*, 2006; Barichivich *et al.*, 2012). Missing values were imputed using the RegEM algorithm (Schneider, 2001), but grid points with more than three years of missing data were discarded. We quantitatively defined the thermal growing season as the period of the year with daily mean temperatures greater than 5 °C (Table 1), which is a common threshold value for determining the boundaries of the thermal potential growing season at mid and high latitudes (Jones & Briffa, 1995; Frich *et al.*, 2002; Barichivich *et al.*, 2012). The curve-fitting procedure of TIMESAT was applied to smooth the daily mean temperature data and estimate the start (STS), end (ETS) and length (LTS) of this seasonal period using the geographically constant 5 °C threshold (Table 1). The 'intensity' of the thermal growing season, defined here as the time-integrated temperature (TI-TEM) over the growing season, was computed as the sum of smoothed daily mean temperatures between STS and ETS.

We used a validated 25 × 25 km satellite data set of daily landscape (soil, snow, and vegetation) freeze-thaw dynamics (Kim *et al.*, 2011) to estimate the timing and length of the non-frozen season between 1988 and 2007 (Table 1). This data set is based on global microwave observations from morning (am) and afternoon (pm) equatorial crossings of the Special Sensor Microwave Imager (SSM/I). The timing (day of year) of the primary spring thaw (STH) for each 25 km grid box and year was estimated from the daily combined parameter as the first day when at least 12 out of 15 consecutive days were classified as non-frozen (am and pm thawed) between January and June (Kim *et al.*, 2012), whereas the timing of the autumn freeze (AFZ) was estimated following the same procedure for frozen days (a.m. and p.m. frozen) between September and December. The length of the non-frozen season (LNF) was then defined as the number of days between STH and AFZ.

In addition, we derived a daily freeze-thaw classification between 1950 and 2011 based on gridded minimum and maximum air temperatures from the HadGHCND data set to investigate the large-scale consistency of the satellite observations and long-term trends in freeze-thaw dynamics. Thawed and frozen days were defined as days with minimum air temperatures above and below 0 °C, respectively.

Finally, to assess the relationship between snow-cover and the timing of spring thawing and start of the thermal growing season, we estimated the timing of spring snow melt (SMT) over the continuous period 1972–2011 from the satellite-based weekly gridded snow-cover data set maintained by the Rutgers University Global Snow Lab (Robinson *et al*., 1993). The date of snow melt was defined as the first week of a continuous run of 5 weeks without snow between January and June.

Atmospheric CO_2

The seasonal signature in the atmospheric concentration of CO_2, which reflects the changing balance between photosynthesis and respiration of ecosystems through the year, has commonly been used to infer the seasonal course of the net carbon exchange between the terrestrial biosphere and the atmosphere (i.e. net ecosystem productivity – NEP; Houghton, 1987; Keeling *et al*., 1996; Piao *et al*., 2008). Previous studies have shown that the annual cycle of atmospheric CO_2 at high northern latitudes is dominated largely by the metabolism of northern terrestrial ecosystems, with minimal impacts from ocean exchange, fossil fuel emissions, and tropical biomass burning (Randerson *et al*., 1997; Piao *et al*., 2008). Hence, we used long-term monthly observations of atmospheric CO_2 concentration at Point Barrow (71°N), Alaska, over the period 1972–2010 (GLOBALVIEW-CO2, 2011) to assess the influence of changes in the growing season on the land-atmosphere net carbon exchange. This is the longest continuous record of background CO_2 concentration at northern latitudes and integrates the net seasonal flux of carbon from all land regions north of 40°N, though with a larger regional contribution from fluxes near the station in Alaska (Kaminski *et al*., 1996).

As in earlier studies (e.g., Buermann *et al*., 2007; Barichivich *et al*., 2012), we applied the data filtering technique of Thoning *et al*. (1989) to the monthly time series of flask CO_2 observations to isolate the detrended smoothed annual cycle and extract metrics for the peak-to-trough amplitude and phasing (zero-crossing dates in spring and autumn) of the annual cycle of CO_2 (Table 1). The peak-to-trough amplitude provides a measure of the relative magnitude of net photosynthetic carbon uptake by terrestrial ecosystems (photosynthesis CO_2 uptake minus CO_2 release from ecosystem respiration and disturbance) over the period when photosynthesis exceeds ecosystem respiration, running from the start of the growing season until the day when minimum CO_2 is reached (Keeling *et al*., 1996; Buermann *et al*., 2007). Thus, variations in CO_2 amplitude largely reflect changes in photosynthesis (net CO_2 uptake) over the course of the growing season in the north. The spring (SZC) and autumn (AZC) zero-crossing dates are surrogates for the respective onset and termination of the net carbon uptake period (Keeling *et al*., 1996; Piao *et al*., 2008; Barichivich *et al*., 2012), which is affected by changes in the seasonal timing of the growing season.

To test the large-scale validity of the CO_2 observations at Point Barrow, time series of zero-crossing dates and annual amplitude were also derived from monthly zonal-mean CO_2 concentrations north of 60°N from the reference marine boundary layer matrix of GLOBALVIEW-CO2 (2011) over the period 1979–2010.

Intercomparison and statistical analysis

A summary of the parameters used to characterize the potential and photosynthetic growing season is given in Table 1. All the parameters were converted to anomalies with respect to their common period 1988–2007 and then spatially averaged over North America, Eurasia, and the entire circumpolar region north of 45°N.

The temporal agreement among the continental and circumpolar estimates of timing and length of the non-frozen season and the photosynthetic and thermal growing seasons was examined using the Kendall coefficient of concordance (*W*; Legendre, 2010) and linear correlation analysis over the common period 1988–2007. *W* is a nonparametric measure of correlation among three or more variables and varies between 0 (no association) and 1 (perfect association). The statistical significance of *W* was estimated using a permutation test with 10 000 simulations (Oksanen *et al*., 2011). The significance of correlations was estimated using a nonparametric random phase test with 1000 Monte-Carlo simulations (Ebisuzaki, 1997), which is robust to autocorrelation in the series. Trend analysis was carried out using the nonparametric Mann–Kendall trend test implemented in the zyp package in R statistics (Bronaugh, 2009).

We examined the response of growing season photosynthetic activity to temperature changes by comparing the seasonal integrals of NDVI (TI-NDVI) and temperature (TI-TEM) over the period 1982–2011. The influence of changes in the timing of the growing season on the timing of net carbon uptake by northern ecosystems was assessed by comparing the zero-crossing dates (SZC, AZC) at Point Barrow with the timing of the non-frozen season and the thermal and photosynthetic growing seasons over the common period 1988–2007. We also compared the seasonal NDVI integral with the amplitude of the annual cycle of CO_2 (AMP) at Point Barrow to assess the linkages between variations in gross photosynthesis and changes in the magnitude of net carbon uptake by northern ecosystems.

Results

Timing

Figure 1 compares continental and circumpolar time series of anomalies in the timing and length of the non-frozen season and the photosynthetic and thermal growing seasons covering different periods between 1950 and 2011. The spatially averaged anomalies agree

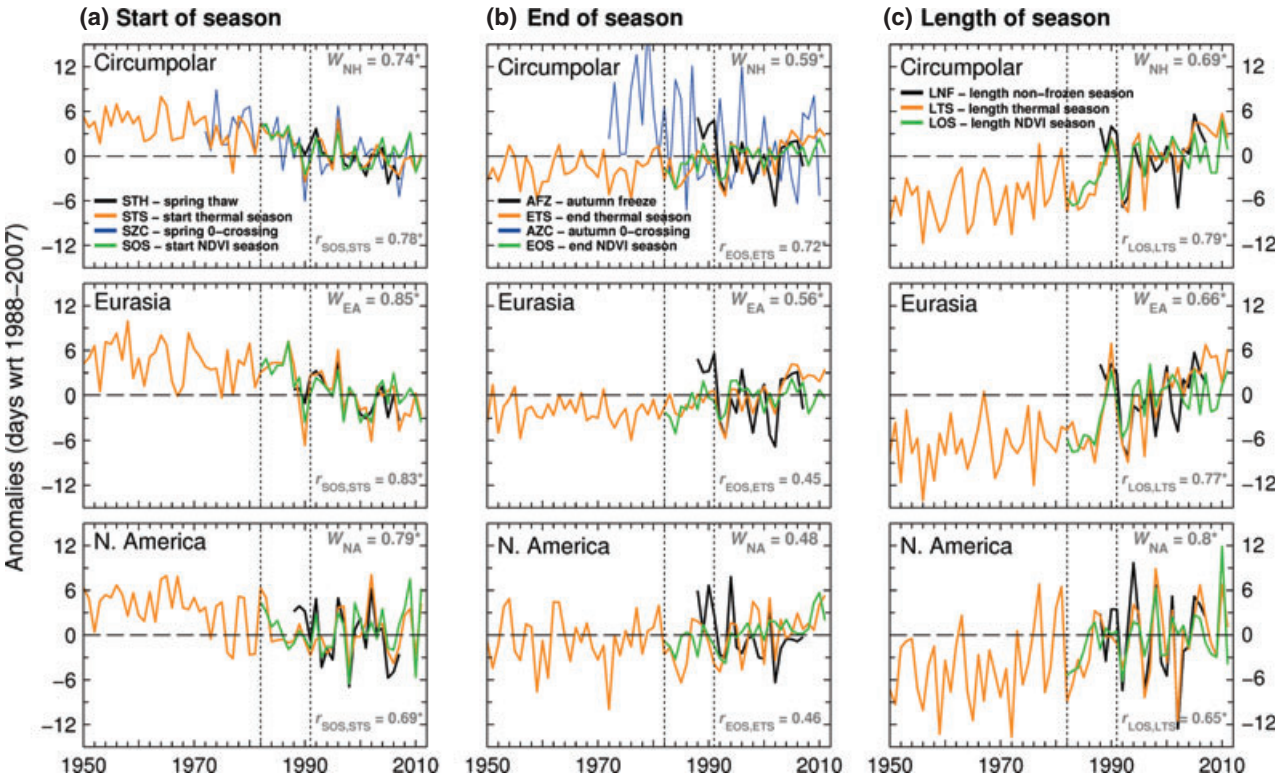

Fig. 1 Circumpolar and continental variations in the timing (a, b) and length (c) of the growing season at latitudes north of 45°N and CO_2 zero-crossing dates at Point Barrow. The *W* statistic for each parameter and spatial domain provides a measure of the temporal consistency among variations in non-frozen season and thermal and photosynthetic growing seasons over the period 1988–2007. The correlation between variations in corresponding series of photosynthetic and thermal growing season over the period 1982–2011 is shown in the lower right corner of each panel. An asterisk denotes significance at the $P < 0.05$ level. The vertical dotted lines indicate the eruptions El Chichón in 1982 and Mount Pinatubo in 1991.

remarkably well in spring on a continental ($W_{EA} = 0.85$, $W_{NA} = 0.79$, $P < 0.05$) and circumpolar ($W_{NH} = 0.74$, $P < 0.05$) scale (Fig. 1a), indicating a strong synchrony between variations in the timing of the spring thaw (STH) and the start of the thermal (STS) and photosynthetic (SOS) growing seasons. Continental and circumpolar anomalies in spring thaw are highly correlated with anomalies in the start of the photosynthetic and thermal growing seasons, particularly over Eurasia (Table 2). This indicates a strong springtime coupling between the start of the potential (STH and STS) and the photosynthetic growing season at northern latitudes.

The timing of the start of the photosynthetic growing season based on GIMMS NDVI3g is highly consistent with estimates based on the previous NDVIg dataset ($r = 0.95$–0.98 for 1982–2006; Fig. S2) and on higher quality MODIS NDVI data ($r = 0.50$–0.88 for 2001–2011; Fig. S3), so our estimates of variations in spring canopy green-up are robust to uncertainties due to differences in satellite sensors and data processing. However, in spite of our efforts to minimize the influence of snow dynamics on the phenological retrievals, snow melt variations may still affect the green-up signal retrieved from NDVI, though snow melt and the onset of photosynthetic activity would be expected to covary significantly at northern latitudes because of their strong common temperature control (Fig. S4).

The phenological series shown in Fig. 1a (STH, SOS, STS) depict a consistent circumpolar trend toward earlier growing seasons. Trend analysis indicates that the circumpolar start of the thermal growing season has advanced significantly by 6.8 days since 1950 at a rate of -1.10 ± 0.28 days per decade^{-1}(Table 3). This long-term advance has been stronger and more sustained in Eurasia (-1.28 ± 0.39 days decade^{-1}, $P < 0.01$) than in North America (-0.93 ± 0.47 days decade^{-1}, $P < 0.01$), where the spring advance halted in the early 1990s (Fig. 1a). This change over North America has resulted in contrasting continental trends during the satellite period between 1982 and 2011. In North America, neither the start of the thermal or the photosynthetic growing seasons has changed significantly since 1982 (Table 3). In contrast, over Eurasia both the thermal and photosynthetic growing seasons have begun significantly earlier since 1982 by 6.9 days (-2.3 ± 0.97 days

Table 2 Correlation matrix of timing and length of the non-frozen season (STH, AFZ, LNF), thermal growing season (STS, ETS, LTS), photosynthetic growing season (SOS, EOS, LOS) and CO_2 zero-crossing dates (SZC, AZC) at Point Barrow over the period 1988–2007

	Start				End				Length	
Variable	STH	STS	SZC		AFZ	ETS	AZC		LNF	LTS
Circumpolar										
STH	·			AFZ	·					
STS	**0.73**	·		ETS	0.44	·		LNF	·	
SZC	**0.53**	**0.65**	·	AZC	−0.24	**−0.58***	·	LTS	**0.74**	·
SOS	**0.66**	**0.67**	0.43	EOS	0.16	**0.74**	**−0.26**	LOS	0.46	**0.74**
Eurasia										
STH	·			AFZ	·					
STS	**0.75***	·		ETS	**0.57**	·		LNF	·	
SZC	**0.45**	**0.55**	·	AZC	−0.14	**−0.35**	·	LTS	**0.56**	·
SOS	**0.78**	**0.77**	0.34	EOS	0.21	**0.57**	**-0.31**	LOS	0.40	**0.78**
North America										
STH	·			AFZ	·					
STS	**0.71**	·		ETS	0.33	·		LNF	·	
SZC	0.38	0.30	·	AZC	**−0.40**	**−0.68***	·	LTS	**0.82**	
SOS	**0.71**	**0.58**	0.23	EOS	−0.10	0.33	−0.11	LOS	**0.63**	**0.58**

Values in bold are significant at $P < 0.05$.
*$P < 0.01$.

Table 3 Mann–Kendall linear trends (± 1 SE) in timing and length of the thermal and photosynthetic growing season from 1982 to 2011 (see Table 1 for acronyms). Trends in the thermal growing season over the longer 1950–2011 period are given in brackets

	Start (days decade^{-1})		End (days decade^{-1})		Length (days decade^{-1})	
Region	STS	SOS	ETS	EOS	LTS	LOS
Circumpolar	**−1.64 ± 0.71***	**−1.11 ± 0.88**	**1.87 ± 0.76***	**0.97 ± 0.61**	**3.50 ± 1.33***	**2.24 ± 1.24***
	(−1.10 ± 0.28*)		**(0.74 ± 0.29*)**		**(1.72 ± 0.48*)**	
Eurasia	**−2.30 ± 0.97***	**−1.78 ± 1.06***	**1.65 ± 0.67***	0.78 ± 0.77	**4.21 ± 1.33***	**2.47 ± 1.21***
	(−1.28 ± 0.39*)		**(0.72 ± 0.31*)**		**(2.06 ± 0.55*)**	
North America	0.16 ± 1.26	0.14 ± 1.53	**1.99 ± 1.29***	**1.32 ± 0.75***	2.08 ± 2.18	0.96 ± 1.42
	(−0.93 ± 0.47*)		(0.42 ± 0.49)		**(1.33 ± 0.71*)**	

Values in bold are significantly different from zero at $P < 0.05$.
*$P < 0.01$.

decade^{-1}, $P < 0.01$) and 5.3 days (−1.78 ± 1.06 days decade^{-1}, $P < 0.01$), respectively. Nevertheless, there is some indication that these advancing trends have weakened during the 2000s (Fig. 1a).

In contrast to spring, Fig. 1b shows that the overall agreement between anomalies in the timing of the AFZ and the end of the photosynthetic (EOS) and thermal (ETS) growing seasons is weaker on both circumpolar ($W_{NH} = 0.59$, $P < 0.05$) and continental ($W_{EA} = 0.56$, $P < 0.05$; $W_{NA} = 0.48$, $P > 0.05$) scales. The agreement is particularly low in North America, where none of the variables (AFZ, EOS and ETS) is significantly correlated with any other (Table 2). This poor general agreement suggests a decoupling between the termination of the potential (AFZ, ETS) and the photosynthetic (EOS) growing season.

The two GIMMS NDVI data sets produce very similar variability in the timing of the termination of the photosynthetic growing season ($r = 0.85$–0.91 for 1982–2011), but the earlier data set (NDVIg) tends to produce stronger autumn delay since around 2003, likely due to calibration issues (Fig. S2). During the past decade, estimates based on GIMMS NDVI3g are less consistent with MODIS NDVI data ($r = 0.25$–0.51 for 2001–2011) than for the start of the growing season, although the overall difference between the data sets is related to disagreements only during 2001 and 2011 (Fig. S3).

There is a general delay in the timing of the end of the thermal and photosynthetic growing seasons during our study period (Table 3). Most of this delay has occurred only during the second half of the 2000s, when a rapid step change took place in Eurasia and to a lesser extent in North America (Fig. 1b). This has resulted in a significant trend toward delayed termination of the thermal growing season in Eurasia by about 4.9 days (1.65 ± 0.67 days decade^{-1}, $P < 0.01$) over the period 1982–2011 (Table 3). The change was smaller for the termination of the photosynthetic growing season and the trend since 1982 is not significant. In North America, the terminations of the thermal and photosynthetic growing seasons have both been delayed significantly since 1982 by 6 and 4 days at linear rates of 1.99 ± 1.29 and 1.32 ± 0.75 days decade^{-1}, respectively. These continental-scale changes have resulted in a circumpolar delay in the termination of the thermal growing season of 5.6 days (1.87 ± 0.76 days decade^{-1}, $P < 0.01$) but only 2.9 days in the termination of the photosynthetic growing season since 1982 (0.97 ± 0.61 days decade^{-1}, $P < 0.05$). Thus, these results indicate that the autumnal extension of the thermal potential growing season since 1982 has been nearly twice that of the photosynthetic growing season.

Length

Figure 1c shows that the lengths of the non-frozen season (LNF) and the thermal (LTS) and photosynthetic (LOS) growing seasons have increased steadily since the early 1980s in Eurasia, while in North America there has been no overall increase during this period. The overall agreement in the temporal anomalies of the three variables is significant and stronger in North America ($W_{NH} = 0.69$, $W_{EA} = 0.66$, $W_{NA} = 0.80$, $P < 0.05$), where all three variables are significantly correlated with each other (Table 2). There is also a consistent pattern of temporal variability in the length of the photosynthetic growing season between the GIMMS NDVI datasets and MODIS NDVI data (Figs S2 and S3).

Trend analysis indicates that in Eurasia the thermal and photosynthetic growing seasons have lengthened by 12.6 and 7.4 days since 1982, with respective linear rates of 4.21 ± 1.33 and 2.47 ± 1.21 days decade^{-1} (Table 3). Thus, the lengthening of the thermal growing season has been almost twice that of the photosynthetic growing season. Clearly, this pattern of lengthening has been dominated by spring advance (Fig. 1a) and the large difference in trends occurs because of a smaller rate of delay in the termination of the photosynthetic growing season.

In North America, the thermal and photosynthetic growing seasons have not lengthened during this period, largely because of the pause in the spring advance in the early 1990s. Yet, the thermal growing season has lengthened significantly since 1950, but primarily because of the spring advance prior to the 1990s (Table 3). On a circumpolar scale, the lengthening of the thermal growing season since 1982 has been substantially larger than that of the photosynthetic growing season, with respective changes of 10.5 and 6.7 days and linear rates of 3.50 ± 1.33 and 2.24 ± 1.24 days decade^{-1} (Table 3).

The continental and circumpolar rates of lengthening of the thermal growing season over the full record from 1950 to 2011 shown in Table 3 (1.33 to 2.06 days decade^{-1}) agree closely with the rates of increase (1.41 to 2.03 days decade^{-1}) in the annual number of non-frozen days derived from minimum surface air temperatures from the same data set shown in Fig. 2. This indicator of non-frozen days is roughly equivalent to the length of the continuous non-frozen season (LNF) and is strongly correlated with SSM/I satellite microwave observations of landscape freeze-thaw dynamics between 1988 and 2007. As shown in Fig. 2, the strength of the correlation varies from 0.75 ($P < 0.05$)

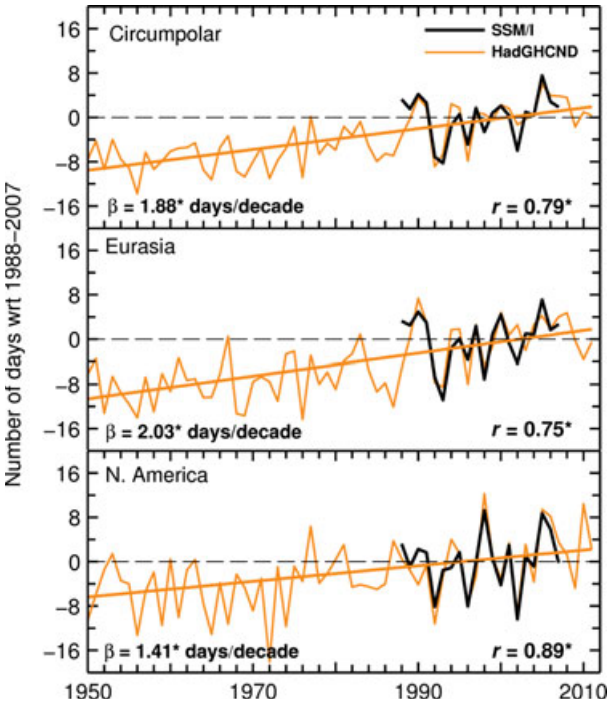

Fig. 2 Changes in annual number of non-frozen days estimated from satellite microwave (SSM/I) and from gridded surface air temperature observations (HadGHCND) north of 45°N. Correlations between the satellite and temperature-based series for the period 1988-2007 and linear trends (β) for HadGHCND series over the 1950-2011 period are given in each panel. An asterisk denotes significance at the $P < 0.05$ level.

over Eurasia to 0.89 ($P < 0.05$) in North America and 0.79 ($P < 0.05$) on a circumpolar scale. The correlations are also high for the number of non-frozen days during spring and autumn (Fig. S5).

This strong agreement validates the satellite landscape freeze-thaw record, and the close relationship with the indicator of non-frozen days based on minimum temperatures enables us to estimate long-term changes in the non-frozen season from 1950 to the present. During this 62-year period, the annual number of non-frozen days has increased significantly by 12.6 days in Eurasia and 8.7 days in North America (Fig. 2). This compares well with a concurrent lengthening of the thermal growing season by 12.7 days (2.06 ± 0.55 days decade^{-1}, $P < 0.01$) in Eurasia and 8.2 days (1.33 ± 0.71 days decade^{-1}, $P < 0.01$) in North America (Table 3). On a circumpolar scale, the increase in the annual number of non-frozen days has been 11.7 days during the same period, which is similar to a lengthening of the thermal growing season of 10.7 days (1.72 ± 0.48 days decade^{-1}, $P < 0.01$). Seasonally, the increase in non-frozen days is significant in both spring (0.77–1.07 days decade^{-1}) and autumn (0.62–0.66 days decade^{-1}), but the stronger increase has occurred in spring (Fig. S5).

Intensity

Figure 3a compares the spatially averaged time series of cumulative growing season NDVI (TI-NDVI) and temperature (TI-TEM). The agreement between these two variables is very good, with correlation values ranging from 0.68 ($P < 0.05$) in North America to 0.81 ($P < 0.05$) in Eurasia and 0.80 ($P < 0.05$) on a circumpolar scale. The correlations remain statistically significant even after removing the trend from the series by applying a high-pass filter (Fig. S6). Thus, there is a strong indication that cumulative thermal growing season temperature drives most of the interannual and long-term variations in growing season photosynthetic activity over the study domain.

The large-scale patterns of cumulative growing season NDVI are consistent between the two GIMMS NDVI datasets, but NDVIg shows a more negative trend than NDVI3g over the period 1982–2006 (Fig. S2). In the most recent decade, GIMMS NDVI3g agrees reasonably well with MODIS NDVI data (Fig. S3), indicating a common large-scale vegetation signal between the AVHRR and MODIS sensors during recent years.

Neither the continental nor the circumpolar series of cumulative thermal growing season temperatures (TI-TEM) shows any significant warming during the three decades prior to the start of the satellite NDVI record in 1982. Shortly after this date, thermal growing season temperatures and photosynthetic intensity (TI-NDVI) increased, especially after around 1988, then decreased temporarily during 1992 and 1993 because of the transient spring and summer cooling induced by the eruption of Mount Pinatubo in 1991, and continued to rise thereafter. The rate of growing season warming

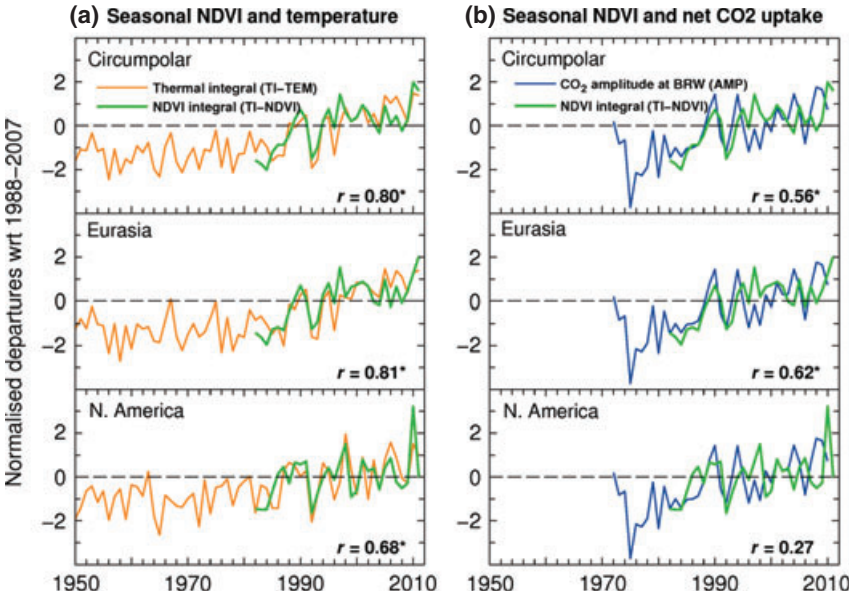

Fig. 3 Comparison of variations in seasonally integrated NDVI with seasonally integrated temperature (a), and peak-to-trough amplitude of the annual cycle of atmospheric CO_2 at Point Barrow (b). The correlation between the series over their common period is shown in each panel. An asterisk denotes significance at the $P < 0.05$ level.

and photosynthetic greening trends weakened after the mid-1990s until the increases that occurred in the final two years of the record (2010 and 2011). The warming and greening trends are stronger in Eurasia than in North America and the circumpolar average is dominated by changes over Eurasia.

A prominent feature in the NDVI record is the very intense photosynthetic growing season in North America during 2010, with an anomaly about three SD above the mean (Fig. 3a). This continental anomaly is also shown by MODIS NDVI (Fig. S3) and was dominated by a strong seasonal greening in eastern North America, in connection with a concurrent pattern of strong seasonal warming (Fig. 4). These anomalies are also consistent with an abrupt advance of about 6 days in the start of the thermal and photosynthetic seasons over North America in 2010 (Fig. 1a).

Correlation with atmospheric CO_2 annual cycle

Temporal variations in the amplitude and phase (zero-crossing dates) of the annual cycle of atmospheric CO_2 based on flask observations at Point Barrow are strongly correlated ($r > 0.71$, $P < 0.05$, 1979–2010) with those based on zonally averaged CO_2 concentrations in the marine boundary layer north of 60°N (Fig. S7), indicating that this station record is representative of the northern latitudes. However, note that these two CO_2 records are not completely independent as the observations at Point Barrow are also included in the zonal averages.

Variations in the timing of the spring thaw (STH) and the start of the thermal (STS) and photosynthetic (SOS) growing seasons are positively correlated with anomalies in spring CO_2 zero-crossing date (SZC) at Point Barrow (Table 2). Though the correlations with the start of the photosynthetic growing season are not significant ($P < 0.05$) over the period 1988–2007, the circumpolar trend toward earlier growing seasons is consistent with an advance of 5.7 days (-1.45 ± 0.84 days decade^{-1}, $P < 0.01$) in the timing of spring CO_2 zero-crossing date since 1972 (Fig. 1a).

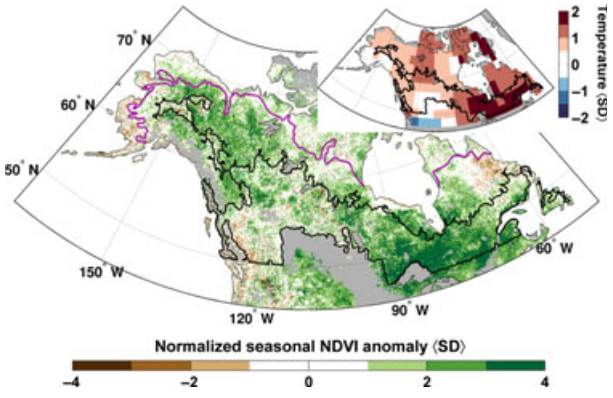

Fig. 4 Spatial pattern of normalized anomalies of seasonally integrated NDVI (TI-NDVI) and temperature (TI-TEM) in North America during 2010. Inland water bodies, croplands, urban and barren or sparsely vegetated regions are shaded gray. The black polygon represents the extent of the continuous needleleaf boreal forest and the purple line indicates the position of the Arctic treeline.

In contrast, variations in the timing of the AFZ and end of the photosynthetic (EOS) and thermal (ETS) growing seasons are all negatively correlated with the timing of the autumn CO_2 zero-crossing date (AZC) at Point Barrow (Fig. 1b and Table 2). However, the significance of the correlations varies substantially and the magnitudes are weaker than during spring. The timing of the autumn zero-crossing date at Point Barrow shows very large year-to-year variability and has advanced by about 6.3 days (-1.61 ± 1.53 days decade^{-1}, $P < 0.05$) since 1972, offsetting the concurrent advance in the spring zero-crossing date (5.7 days). This coincides with a general delay in the termination of the thermal and photosynthetic growing seasons (Table 3). These inverse relationships indicate that unlike in spring, an extension of the potential and photosynthetic growing season in autumn tends to be associated with earlier rather than delayed termination of the period of net ecosystem carbon uptake at northern latitudes. Nevertheless, contrary to the negative relationship observed during the entire period, the autumnal extensions of the thermal and photosynthetic growing seasons in the mid-2000s have been mostly associated with a delayed termination of the period of net ecosystem carbon uptake (Fig. 1b).

Figure 3b shows that the intensity of the photosynthetic growing season (TI-NDVI) is positively correlated with the peak-to-trough amplitude (AMP) of the annual cycle of atmospheric CO_2 at Point Barrow. The correlations over the period 1982–2010 range from 0.27 ($P < 0.05$) in North America to 0.62 ($P < 0.05$) in Eurasia and 0.56 ($P < 0.05$) on a circumpolar scale. However, after removing the trend in the series, only the correlation coefficient for Eurasia ($r = 0.45$, $P < 0.05$) is significant (Fig. S6). The continental contrast in the magnitude and significance of the correlations indicates that changes in CO_2 amplitude at this station are dominated by photosynthetic activity in Eurasia. Spatial correlations indicate that photosynthetic activity over most of Alaska is also significantly correlated with variations in CO_2 amplitude at Point Barrow (Fig. S8).

The temperature-driven greening trend in Eurasia is consistent with a long-term increase in peak-to-trough CO_2 amplitude of 22.2% ($P < 0.01$, 1972–2010) relative to the mean of the period 1972–1980. This increase in amplitude has been dominated by a concurrent trend

toward lower summer minimum CO_2 concentrations of 24.9% ($P < 0.01$, 1972–2010) due to enhanced growing season net CO_2 uptake, while the seasonal maximum CO_2 concentrations show no long-term changes (Fig. S7). However, variations in seasonal maximum CO_2 concentrations, and hence variations in wintertime ecosystem respiration, have increasingly influenced the amplitude of the CO_2 annual cycle during most of the 2000s, reducing the correlation with interannual variations in seasonally integrated NDVI (Fig. 3b, Fig. S6).

Discussion

Synchrony of climate and phenological changes during spring and autumn

This study presents a combined assessment of continental and circumpolar changes in potential and photosynthetic growing seasons, inferred from multiple ground and satellite observations of vegetation greenness, surface air temperature, snow-cover and freeze-thaw dynamics covering different periods from 1950 to 2011. Our results show that variations in the timing of the remotely sensed photosynthetic growing season are tightly coupled with the timing of the climatically defined potential growing season in spring but not in autumn (Fig. 1), suggesting a seasonal asymmetry in the phenological response to climate variability at these large spatial scales.

The winter-to-spring transition at northern latitudes is both rapid and dramatic. Typically, before the seasonal thaw, daily solar radiation is already abundant but vegetation metabolism is limited by frozen soils. Thus, rising temperatures strongly stimulate and synchronize the landscape thaw and the onset of vegetation photosynthetic activity (Goulden *et al*., 1998; Jarvis & Linder, 2000), which in turn trigger the greening of the landscape observed by satellites (Myneni *et al*., 1997). The pivotal role played by temperature in these interrelated processes explains the remarkable agreement observed in the vegetation, cryospheric and thermal phenological parameters in spring. Nevertheless, spring snow melt produces a similar increase in NDVI as that produced by vegetation greening (Dye & Tucker, 2003; Delbart *et al*., 2006) and despite efforts to minimize the influence of snow dynamics on phenological retrievals, the potential remaining influence of the snow melt signal on NDVI data may also contribute to this agreement.

The poor autumnal synchrony between thermal, cryospheric and vegetation transitions indicates that autumn senescence, as measured by canopy greenness, is less sensitive to temperature variability than is spring green-up. Autumn senescence is a complex biophysical process triggered by leaf-specific maturation processes and cumulative environmental constraints such as photoperiod, temperature, and soil moisture (Kozlowski & Pallardy, 1997; Rosenthal & Camm, 1997; Vitasse *et al*., 2009; Warren *et al*., 2011; Dragoni & Rahman, 2012). Although the relative importance of these factors is still not well understood (Richardson *et al*., 2013), it has been shown that late-season photosynthetic activity and growth cessation in temperate and boreal regions can be strongly constrained by photoperiod (Suni *et al*., 2003; Kimball *et al*., 2004; Barr *et al*., 2009; Bauerle *et al*., 2012). This sensitivity of autumn phenology to photoperiod is consistent with the evidence for autumnal decoupling shown here between continental-scale variations in the timing of canopy senescence and thermal and cryospheric transitions. To some extent, our use of a fixed 5 °C threshold to define the end of the thermal growing season might also contribute to this autumnal mismatch, as temperature thresholds for late-season vegetation growth may vary considerably with vegetation type and latitude (Piao *et al*., 2006). Nevertheless, the lack of correlation between variations in the timing of vegetation senescence and the autumn freeze (Table 2) provides independent evidence for a decoupling between autumn phenology and thermal conditions. As the influence of photoperiod does not change from year to year, interannual and longer term variability of late-season canopy greenness and the timing of autumn senescence at northern latitudes is still correlated with temperature but less so than during spring (Estrella & Menzel, 2006; Jeong *et al*., 2011; Piao *et al*., 2011; Zeng *et al*., 2011; Dragoni & Rahman, 2012; Zhu *et al*., 2012).

Changes in potential and photosynthetic growing seasons

An examination of variations in the thermal growing season (Fig. 1) and the frequency of temperature-based non-frozen days back to 1950 (Fig. 2b) indicates that neither the length nor the timing of the termination of the potential growing season has changed significantly in the period prior to the satellite era (1950–1981). Nevertheless, there is evidence for a nearly hemispheric-wide advance in the start of the potential growing season since the early 1970s. This is characterized by advanced thermal growing seasons (Fig. 1a), earlier snow melt (Fig. S4) and increased frequency of non-frozen days in spring (Fig. S5). The spring advance and the associated trend toward earlier snow melt have continued until the present in Eurasia but halted in North America in the early 1990s. These changes have resulted in a circumpolar advance of the thermal growing season of about 6.8 days since 1950 and a similar increase in non-frozen days in spring of 6 days. This

finding is consistent with previous studies showing a shift by 7.3 days in the timing of spring land surface temperatures north of 20°N from 1960 to 2009 (Burrows *et al.*, 2011), advanced timing of the last day below 5 °C by 6.7 days from 1955 to 2002 (Schwartz *et al.*, 2006) and a general advance in the timing of spring phenological events of animal and plant species over the last half-century (Parmesan & Yohe, 2003).

The extended historical context of our multiple-parameter assessment shows that the potential growing season has undergone unprecedented changes during the satellite era (1982–2011) as a result of the rapid warming observed throughout most of the northern latitudes (Fig. 1 and 3a). Nearly, all of the circumpolar lengthening of the thermal growing season since 1950 (10.7 days) has occurred during the satellite period (10.5 days), with a similar extension in spring (4.9 days) and autumn (5.6 days). This is in close agreement with the widespread reduction of low temperature constraints on plant growth (Bunn *et al.*, 2007; Zhang *et al.*, 2008) and lengthening of the potential growing season observed at high latitudes during the past 30 years of continuous satellite observation of the cryosphere (McDonald *et al.*, 2004; Smith *et al.*, 2004; Zhang *et al.*, 2011; Kim *et al.*, 2012).

The NDVI-based photosynthetic growing season of northern vegetation has responded significantly to the rapid lengthening and warming of the potential growing season during the satellite period (Figs 1c and 3a). This response is consistent with earlier remote sensing and modeling studies showing a progressive lengthening of the photosynthetic growing season and large-scale greening trends across most of the northern latitudes (e.g., Myneni *et al.*, 1997; Tucker *et al.*, 2001; Zhou *et al.*, 2001; Lucht *et al.*, 2002; Euskirchen *et al.*, 2006; Piao *et al.*, 2007; Bhatt *et al.*, 2010; Beck & Goetz, 2011; Jeong *et al.*, 2011). However, a new finding of this study is that the circumpolar lengthening of the photosynthetic growing season over the satellite period has been substantially smaller than the lengthening of the thermal potential growing season, owing to a twofold autumnal extension of the latter (Table 3). During the period 1982–2011, the thermal growing season lengthened by 10.5 days (owing to an extension of 4.9 days in spring and 5.6 days in autumn), whereas the photosynthetic growing season lengthened by 6.7 days in the same period (owing to an extension of 3.3 days in spring and 2.9 days in autumn). Admitting data and methodological uncertainties, these trends suggest that unlike in spring the photosynthetic growing season has not tracked the extension in the thermal potential growing season in autumn, when photosynthesis and canopy greenness become more limited by factors other than temperature (Kozlowski & Pallardy, 1997; Rosenthal & Camm, 1997; Dye & Tucker, 2003; Piao *et al.*, 2011; Warren *et al.*, 2011). A recent study based on a slightly extended version of the GIMMS NDVIg data set from 1982 to 2008 (Jeong *et al.*, 2011) highlighted a hemispheric lengthening of the NDVI-based growing season (10.5 days) driven primarily by an autumnal (7.6 days) rather than a spring extension (3.5 days). So, even though these authors found a spring extension similar to our study (3.3 days), they estimated a more than twofold extension in autumn (2.9 vs. 7.6 days). We have shown that phenological variations based on GIMMS NDVIg and the newer NDVI3g data set are highly consistent, except for a substantially stronger autumn delay in the NDVIg data set since around 2003 (Fig. S2). The general agreement between the phenological parameters based on the NDVI3g data set and Terra MODIS NDVI data during the past decade (Fig. S3) suggests that the discrepancy between the results presented here and those of Jeong *et al.* (2011) could be related to calibration issues in the later part of the GIMMS NDVIg data set that may have led to an overestimation of autumnal trends. Differences in the methodologies employed to compute phenology may further contribute to the different inferences between these studies. The analysis of other NDVI data sets and alternative vegetation indices (Huete *et al.*, 2002; Jones *et al.*, 2011; Liu *et al.*, 2011) should shed more light on the significance of this apparent autumnal decoupling between northern vegetation activity and climate variability.

Large-scale phenological trends during the satellite period (1982–2011) are characterized by a marked continental contrast. Trends in thermal and photosynthetic growing season length and intensity are stronger in Eurasia than in North America (Figs 1 and 3a), consistent with findings of earlier studies (Piao *et al.*, 2007; Jeong *et al.*, 2011; Barichivich *et al.*, 2012). The springtime extension has been greater in Eurasia, whereas the autumnal extension has been larger in North America. As in the circumpolar average, the lengthening of the thermal growing season in Eurasia (12.6 days) has been substantially larger than that of the photosynthetic growing season (7.4 days) because of a smaller autumnal extension of the latter (Table 3). The same pattern of greater lengthening of the thermal growing season occurs in North America. However, unlike in Eurasia, neither the thermal nor the photosynthetic growing season has lengthened significantly, despite significant autumnal extensions (Table 3). Earlier studies have shown that these contrasting continental trends are consistent with differences in the magnitude and timing of the seasonal warming over the two continents, and are mostly related to the more rapid rise of spring temperatures in Eurasia and of autumn temperatures in North

America (Piao *et al.*, 2007, 2008; Wang *et al.*, 2011; Barichivich *et al.*, 2012). Regional increases in the frequency and severity of droughts (Dai, 2011), fire and insect disturbances (Westerling *et al.*, 2006; Kurz *et al.*, 2008), feedbacks from declining snow-cover extent and melting permafrost (Callaghan *et al.*, 2011), and compositional and structural vegetation changes (Elmendorf *et al.*, 2012) are also likely to have played an important role on the spatiotemporal variability of these long-term phenological patterns. As a result, phenological trends are highly variable within continents and between biomes, with a strong dependency on vegetation type (Goetz *et al.*, 2005; Jeong *et al.*, 2011).

Recent remote sensing studies based on GIMMS NDVIg data have documented seasonal greenness changes suggesting a relative weakening of the springtime extension and a magnification of the autumnal extension of the photosynthetic growing season at northern latitudes since the early 2000s (Jeong *et al.*, 2011; Piao *et al.*, 2011; Zhu *et al.*, 2012). Similar decadal changes appear in our thermal and NDVI phenological parameters during the past decade (Fig. 1a–b). In particular, the year 2005 saw a step change toward a further extension of the thermal and, to a lesser extent, the photosynthetic growing season in Eurasia (Fig. 1b). Although in North America this change is less obvious, there has also been a conspicuous autumnal extension in the photosynthetic growing season since around 2009.

These decadal phenological changes are consistent with a recent weakening of the long-term warming in winter/spring and a rapid increase in autumn temperatures (Jeong *et al.*, 2011; Barichivich *et al.*, 2012; Cohen *et al.*, 2012). In a companion study (Barichivich *et al.*, 2012), we found that the recent autumnal shift in the thermal growing season was associated with an abrupt autumn warming of about 1 °C at northern latitudes since 2005. This rapid warming has resulted in the longest thermal growing seasons since 1950 over Eurasia and on a circumpolar scale (Fig. 1c). Nevertheless, the magnitude of the concurrent autumnal extension of the photosynthetic growing season has been substantially smaller (Fig. 1b), consistent with the weaker temperature sensitivity of autumn phenology discussed above. However, recent warming-induced increases in fire disturbance and insect defoliation in northern forests (Westerling *et al.*, 2006; Soja *et al.*, 2007; Kurz *et al.*, 2008) may have also influenced the seasonal patterns of vegetation greenness during the past decade (Beck & Goetz, 2011). Also, the magnitude and even the sign of these short-term trends in seasonal greenness have been found to differ substantially between NDVI datasets from different satellite sensors (Zeng *et al.*, 2011; Zhang *et al.*, 2013). Unlike studies based on GIMMS NDVIg data (Jeong *et al.*, 2011; Piao *et al.*, 2011; Zhu *et al.*, 2012), a recent study based on Terra MODIS NDVI for the period 2000–2010 (Zeng *et al.*, 2011) reported a continuous extension of the photosynthetic growing season in spring but no clear extension in autumn over the circumpolar region north of 60°N. This earlier study also found a stronger spring extension (11.5 days decade^{-1}) in North America than in Eurasia (2.7 days decade^{-1}). Such a strong spring extension in North America is inconsistent with our results based on temperature and NDVI3g data through 2011 (Fig. 1). Since we have shown that phenological variations based on GIMMS NDVI3g and Terra MODIS NDVI agree well over the period 2001–2011, particularly in spring (Fig. S3), we conclude that this apparent discrepancy must be related to differences in data processing, spatial domain or the period used for analysis, rather than to any difference in NDVI data sets. This highlights the difficulty of extracting and interpreting meaningful phenological trends from short satellite records.

The variability of seasonally integrated NDVI presents a very consistent picture of vegetation productivity tightly coupled to continental and circumpolar variations in seasonally integrated temperatures during the entire satellite period (Fig. 3a). This is illustrated by the unprecedented increase in seasonally integrated NDVI across the east of North America during the anomalously warm growing season in 2010 (Fig. 4), despite severe canopy damage by a late spring frost event following the exceptionally early leaf-out across the region (Hufkens *et al.*, 2012). A similar correspondence in temperature and NDVI integrals has been reported for the circumpolar tundra region (Bhatt *et al.*, 2010), in agreement with the strong temperature limitation of vegetation productivity at high northern latitudes (Nemani *et al.*, 2003).

Continentally averaged series of NDVI and temperature integrals indicate that the large-scale greening trend observed over northern latitudes during recent decades (Myneni *et al.*, 1997; Zhou *et al.*, 2001) was associated with an abrupt warming of the growing season since the late 1980s, particularly in Eurasia (Fig. 3a). The seasonal warming and associated greening trend paused during the second half of the 1990s and 2000s. Earlier studies based on AVHRR NDVI data have attributed this decadal change in the magnitude of growing season greening to regional changes in temperature, increased summer drought stress and divergent climate responses of tundra and boreal forest biomes (Angert *et al.*, 2005; Goetz *et al.*, 2005; Zhang *et al.*, 2008; Beck & Goetz, 2011; Piao *et al.*, 2011; Wang *et al.*, 2011). However, our results indicate that changes in growing season temperature alone explain most of

this decadal weakening of the greening trend on continental and circumpolar scales. This suggests that other factors such as drought, fire, insect outbreaks, land use change, and nitrogen and CO_2 fertilization may have individually played a smaller role than temperature in influencing continental vegetation productivity integrated over the entire growing season.

Growing season and atmospheric CO_2 annual cycle

It has previously been shown that the extensions of the growing season in spring and autumn have contrasting effects on the net carbon balance of northern ecosystems due to a greater increase in ecosystem respiration over photosynthesis during autumn (Randerson *et al.*, 1999; Piao *et al.*, 2008; Vesala *et al.*, 2010; Barichivich *et al.*, 2012). Nevertheless, net autumnal ecosystem responses are generally less consistent than in spring and increased rather than decreased autumnal net carbon uptake has been observed in some stand-level studies (Richardson *et al.*, 2010; Dragoni *et al.*, 2011). Yet, these opposite net ecosystem responses to changes in the beginning and end of the growing season are a clear large-scale feature of our analysis of the annual cycle of atmospheric CO_2 at Point Barrow. While extensions of the potential and photosynthetic growing seasons in spring are consistently associated with earlier net ecosystem uptake of atmospheric CO_2 (earlier spring CO_2 zero-crossing), an extension in autumn tends to be associated with an earlier rather than a delayed net ecosystem release of CO_2 to the atmosphere (earlier autumn CO_2 zero-crossing).

An important finding of this study is that in Eurasia and North America the autumnal extension of the thermal potential growing season during the satellite period has been substantially larger than that of the photosynthetic growing season. The extended warmth might be expected to have resulted in a substantial stimulation of autumnal ecosystem carbon release and earlier termination of the period of net carbon uptake (i.e., earlier autumn CO_2 zero-crossing), potentially offsetting the spring advance in net carbon uptake period. Indeed, the overall advance in spring CO_2 zero-crossing date at Point Barrow since 1972 (5.7 days) has been offset by a concurrent advance in the autumn zero-crossing date (6.3 days). Yet, the abrupt autumn warming and associated autumnal extension of the potential and photosynthetic growing seasons after 2005 have not been associated with an advance in autumn CO_2 zero-crossing date at Point Barrow as might be expected (Fig. 1b). Instead, the autumn CO_2 zero-crossing has been delayed during this period, suggesting an autumnal extension rather than a shortening of the period of net carbon uptake in recent years. A similar delay in autumn CO_2 zero-crossing during this recent period has been found at several other high-latitude observing stations (Barichivich *et al.*, 2012) and is also apparent in the marine boundary layer CO_2 concentrations (Fig. S5). This anomaly could be in part related to a decrease in ecosystem respiration and to large-scale processes other than the metabolism of terrestrial ecosystems, such as temporal changes in atmospheric transport, ocean uptake, and fossil fuel emissions. It has been shown that atmospheric transport changes can account for up to about 15% of the interannual variability in autumn CO_2 zero-crossing at Point Barrow (Piao *et al.*, 2008). Modeling studies are needed to investigate the relative contribution made by changes in atmospheric transport dynamics and other factors that produced this recent change in autumn CO_2 zero-crossing at northern latitudes after 2005.

Earlier analyses of the annual cycle of atmospheric CO_2 at Point Barrow have shown a consistent increase in the peak-to-trough amplitude (Keeling *et al.*, 1996), associated with the increase in growing season photosynthetic activity, particularly in spring, observed at northern latitudes during the 1980s and 1990s (Myneni *et al.*, 1997; Randerson *et al.*, 1999). Our updated analysis indicates that this increase in amplitude has continued until the present, following the temperature-driven growing season greening over Eurasia (Fig. 3b). Except for Alaska, photosynthetic activity over most of North America seems to have little influence on the amplitude of the annual cycle of atmospheric CO_2 at this station (Fig. S8), consistent with the spatial footprint of the station described by earlier studies (Kaminski *et al.*, 1996; Barichivich *et al.*, 2012). Overall, since 1972, the peak-to-trough CO_2 amplitude has increased significantly by 22.2% with respect to the 1970s as a result of a decreasing trend (24.9%) in summer minimum CO_2 concentrations associated primarily with a shift toward warmer, longer, and more productive growing seasons in Eurasia during the late 1980s. This concurrent large-scale shift in temperature and vegetation greenness at northern latitudes is strongly consistent with earlier evidence for an abrupt increase in the mean of the net land carbon sink by about 1 Pg C yr^{-1} in 1988/1989 (Sarmiento *et al.*, 2010; Beaulieu *et al.*, 2012). More recently, the increased influence of wintertime ecosystem respiration on the seasonal amplitude of the CO_2 annual cycle during most of the 2000s has reduced the correspondence of year-to-year variations in the peak-to-trough CO_2 amplitude and growing season NDVI over Eurasia (Fig. 3b).

A number of studies have shown that summer warming is increasingly associated with reduced rather than increased plant productivity during recent years at mid to high northern latitudes because of increased drought

stress (Angert *et al*., 2005; Ciais *et al*., 2005; Buermann *et al*., 2007; Zhang *et al*., 2008; Peng *et al*., 2011; Piao *et al*., 2011; Ma *et al*., 2012). However, on a continental scale, we do not find clear evidence for reductions in photosynthetic activity integrated over the entire growing season or net CO_2 uptake with recent warming. This may be related to differences in seasonal windows and spatial domains between our own and these earlier studies. Most of the earlier studies are either regional or else they have included the mid-latitudes, where the soil moisture constraint on plant productivity is stronger (Nemani *et al*., 2003).

In conclusion, our assessment of multiple climate and vegetation indicators of growing season changes has revealed a picture of complex and highly dynamical responses of terrestrial ecosystems to the rapid warming over the past three decades at northern latitudes. The net effect of this observed warming has been an increase in the sequestration of atmospheric CO_2 by cool northern terrestrial ecosystems, particularly in Eurasia. The different ecosystem responses at the opposite ends of the growing season, together with the autumnal decoupling between the potential (thermal) and photosynthetic growing seasons have had contrasting effects on the net flux of CO_2 between the terrestrial biosphere and the atmosphere. Determining the impact of continuing 21st century warming on the carbon balance of northern terrestrial ecosystems requires that these complex responses be taken into consideration, including the possibility that the autumn respiration response may become dominant. More detailed studies and ongoing monitoring of vegetation and atmospheric changes will enable better characterization of changes in the growing season and their impacts on terrestrial ecosystems, for specific plant functional types and at both regional and biome scales.

Acknowledgements

We thank Per Jönsson and Lars Eklundh for making available their TIMESAT routine. We also thank Thomas Estilow of the Global Snow Lab at Rutgers University and John Caesar of the Met Office Hadley Centre for providing the most updated snow-cover and temperature data, respectively. JB was supported by doctoral scholarship from the Chilean Government under the program Formación de Capital Humano Avanzado of CONICYT. KRB, TJO, and TMM acknowledge support from UK NERC (under grant NE/G018863/1).

References

Angert A, Biraud S, Bonfils C *et al*. (2005) Drier summers cancel out the CO_2 uptake enhancement induced by warmer springs. *Proceedings of the National Academy of Sciences of the United States of America*, **102**, 10823.

Barichivich J, Briffa KR, Osborn TO, Melvin TM, Caesar J (2012) Thermal growing season and timing of biospheric carbon uptake across the Northern Hemisphere. *Global Biogeochemical Cycles*, **26**, 4015.

Barr A, Black TA, McCaughey H (2009) Climatic and phenological controls of the carbon and energy balances of three contrasting boreal forest ecosystems in Western Canada. In: *Phenology of Ecosystem Processes*, (ed. Noormets A), pp. 3–34. Springer, New York.

Bauerle W, Oren R, Way D *et al*. (2012) Photoperiodic regulation of the seasonal pattern of photosynthetic capacity and the implications for carbon cycling. *Proceedings of the National Academy of Sciences of the United States of America*, **109**, 8612–8617.

Beaulieu C, Sarmiento JL, Fletcher SEM, Chen J, Medvigy D (2012) Identification and characterization of abrupt changes in the land uptake of carbon. *Global Biogeochemical Cycles*, **26**, GB1007.

Beck P, Goetz S (2011) Satellite observations of high northern latitude vegetation productivity changes between 1982 and 2008: ecological variability and regional differences. *Environmental Research Letters*, **6**, 045501.

Beck P, Atzberger C, Høgda K, Johansen B, Skidmore A (2006) Improved monitoring of vegetation dynamics at very high latitudes: a new method using MODIS NDVI. *Remote Sensing of Environment*, **100**, 321–334.

Bhatt U, Walker D, Raynolds M *et al*. (2010) Circumpolar Arctic Tundra Vegetation Change is Linked to sea ice Decline. *Earth Interactions*, **14**, 1–20.

Bronaugh D (2009) *zyp: Zhang + Yue-Pilon Trends Package R Package Version 2.1*. Available at: http://CRAN.R-project.org/package=zyp. (accessed 29 January 2011).

Buermann W, Lintner B, Koven C, Angert A, Pinzon J, Tucker C, Fung I (2007) The changing carbon cycle at Mauna Loa Observatory. *Proceedings of the National Academy of Sciences of the United States of America*, **104**, 4249.

Bunn AG, Goetz SJ, Fiske GJ (2005) Observed and predicted responses of plant growth to climate across Canada. *Geophysical Research Letters*, **32**, L16710.

Bunn AG, Goetz SJ, Kimball JS, Zhang K (2007) Northern high-latitude ecosystems respond to climate change. *Eos*, **88**, 333–335. Available at: www.scopus.com. Cited By (since 1996): 30.

Burrows M, Schoeman D, Buckley L *et al*. (2011) The pace of shifting climate in marine and terrestrial ecosystems. *Science*, **334**, 652–655.

Caesar J, Alexander L, Vose R (2006) Large-scale changes in observed daily maximum and minimum temperatures: creation and analysis of a new gridded data set. *Journal of Geophysical Research*, **111**, D05101.

Callaghan T, Johansson M, Brown R *et al*. (2011) The changing face of arctic snow cover: a synthesis of observed and projected changes. *AMBIO: A Journal of the Human Environment*, **40**, 17–31.

Christidis N, Stott P, Brown S, Karoly D, Caesar J (2007) Human contribution to the lengthening of the growing season during 1950–99. *Journal of Climate*, **20**, 5441–5454.

Ciais P, Reichstein M, Viovy N *et al*. (2005) Europe-wide reduction in primary productivity caused by the heat and drought in 2003. *Nature*, **437**, 529–533.

Cleland E, Chuine I, Menzel A, Mooney H, Schwartz M (2007) Shifting plant phenology in response to global change. *Trends in Ecology & Evolution*, **22**, 357–365.

Cohen J, Furtado J, Barlow M, Alexeev V, Cherry J (2012) Asymmetric seasonal temperature trends. *Geophysical Research Letters*, **39**, L04705.

Dai A (2011) Characteristics and trends in various forms of the Palmer Drought Severity Index during 1900–2008. *Journal of Geophysical Research*, **116**, D12115.

Delbart N, Le Toan T, Kergoat L, Fedotova V (2006) Remote sensing of spring phenology in boreal regions: a free of snow-effect method using NOAA-AVHRR and SPOT-VGT data (1982–2004). *Remote Sensing of Environment*, **101**, 52–62.

Dragoni D, Rahman AF (2012) Trends in fall phenology across the deciduous forests of the Eastern USA. *Agricultural and Forest Meteorology*, **157**, 96–105.

Dragoni D, Schmid H, Wayson C, Potter H, Grimmond C, Randolph J (2011) Evidence of increased net ecosystem productivity associated with a longer vegetated season in a deciduous forest in south-central Indiana, USA. *Global Change Biology*, **17**, 886–897.

Dye D, Tucker C (2003) Seasonality and trends of snow-cover, vegetation index, and temperature in northern Eurasia. *Geophysical Research Letters*, **30**, 1405.

Ebisuzaki W (1997) A method to estimate the statistical significance of a correlation when the data are serially correlated. *Journal of Climate*, **10**, 2147–2153.

Elmendorf SC, Henry GH, Hollister RD *et al*. (2012) Plot-scale evidence of tundra vegetation change and links to recent summer warming. *Nature Climate Change*, **2**, 453–457.

Epstein H, Raynolds M, Walker D, Bhatt U, Tucker C, Pinzon J (2012) Dynamics of aboveground phytomass of the circumpolar arctic tundra during the past three decades. *Environmental Research Letters*, **7**, 015506.

Estrella N, Menzel A (2006) Responses of leaf colouring in four deciduous tree species to climate and weather in Germany. *Climate Research*, **32**, 253.

Euskirchen E, McGuire A, Kicklighter D *et al*. (2006) Importance of recent shifts in soil thermal dynamics on growing season length, productivity, and carbon sequestration in terrestrial high-latitude ecosystems. *Global Change Biology*, **12**, 731–750.

Fensholt R, Proud SR (2012) Evaluation of earth observation based global long term vegetation trends Comparing GIMMS and MODIS global NDVI time series. *Remote Sensing of Environment*, **119**, 131–147.

Frich P, Alexander L, Della-Marta P, Gleason B, Haylock M, Klein Tank A, Peterson T (2002) Observed coherent changes in climatic extremes during the second half of the twentieth century. *Climate Research*, **19**, 193–212.

Friedl M, Sulla-Menashe D, Tan B, Schneider A, Ramankutty N, Sibley A, Huang X (2010) MODIS Collection 5 Global Land Cover: Algorithm Refinements and Characterization of new Datasets. *Remote Sensing of Environment*, **114**, 168–182.

Gao F, Morisette J, Wolfe R *et al*. (2008) An algorithm to produce temporally and spatially continuous MODIS-LAI time series. *IEEE Geoscience and Remote Sensing Letters*, **5**, 60–64.

GLOBALVIEW-CO_2 (2011) *Cooperative Atmospheric Data Integration Project – Carbon Dioxide*. ftp://ftp.cmdl.noaa.gov/ccg/co2/GLOBALVIEW. (accessed 29 June 2011).

Goetz S, Bunn A, Fiske G, Houghton R (2005) Satellite-observed photosynthetic trends across boreal North America associated with climate and fire disturbance. *Proceedings of the National Academy of Sciences of the United States of America*, **102**, 13521.

Goulden M, Wofsy S, Harden J *et al*. (1998) Sensitivity of boreal forest carbon balance to soil thaw. *Science*, **279**, 214.

Grippa M, Kergoat L, Le Toan T, Mognard N, Delbart N, L'Hermitte J, Vicente-Serrano S (2005) The impact of snow depth and snow melt on the vegetation variability over central Siberia. *Geophysical Research Letters*, **32**, L21412.

Houghton R (1987) Terrestrial metabolism and atmospheric CO_2 concentrations. *BioScience*, **37**, 672–678.

Hu J, Moore D, Burns S, Monson R (2010) Longer growing seasons lead to less carbon sequestration by a subalpine forest. *Global Change Biology*, **16**, 771–783.

Huete A, Didan K, Miura T, Rodriguez EP, Gao X, Ferreira LG (2002) Overview of the radiometric and biophysical performance of the MODIS vegetation indices. *Remote Sensing of Environment*, **83**, 195–213.

Hufkens K, Friedl M, Keenan T, Sonnentag O, Bailey A, O'Keefe J, Richardson A (2012) Ecological impacts of a widespread frost event following early spring leaf-out. *Global Change Biology*, **18**, 2365–2377.

James M, Kalluri SN (1994) The Pathfinder AVHRR land data set: an improved coarse resolution data set for terrestrial monitoring. *International Journal of Remote Sensing*, **15**, 3347–3363.

Jarvis P, Linder S (2000) Constraints to growth of boreal forests. *Nature*, **405**, 904–905.

Jeong S, Ho C, Gim H, Brown M (2011) Phenology shifts at start vs. end of growing season in temperate vegetation over the northern hemisphere for the period 1982–2008. *Global Change Biology*, **17**, 2385–2399.

Jones PD, Briffa KR (1995) Growing season temperatures over the former soviet union. *International Journal of Climatology*, **15**, 943–959.

Jones M, Jones L, Kimball J, McDonald K (2011) Satellite passive microwave remote sensing for monitoring global land surface phenology. *Remote Sensing of Environment*, **115**, 1102–1114.

Jönsson P, Eklundh L (2004) TIMESAT–a program for analyzing time-series of satellite sensor data. *Computers & Geosciences*, **30**, 833–845.

Julien Y, Sobrino J (2009) Global land surface phenology trends from GIMMS database. *International Journal of Remote Sensing*, **30**, 3495–3513.

Kaminski T, Giering R, Heimann M (1996) Sensitivity of the seasonal cycle of CO_2 at remote monitoring stations with respect to seasonal surface exchange fluxes determined with the adjoint of an atmospheric transport model. *Physics and Chemistry of the Earth*, **21**, 457–462.

Keeling C, Chin J, Whorf T (1996) Increased activity of northern vegetation inferred from atmospheric CO_2 measurements. *Nature*, **382**, 146–149.

Kim Y, Kimball J, McDonald K, Glassy J (2011) Developing a global data record of daily landscape freeze/thaw status using satellite passive microwave remote sensing. *IEEE Transactions on Geoscience and Remote Sensing*, **49**, 949–960.

Kim Y, Kimball J, Zhang K, McDonald K (2012) Satellite detection of increasing northern hemisphere non-frozen seasons from 1979 to 2008: implications for regional vegetation growth. *Remote Sensing of Environment*, **121**, 472–487.

Kimball J, McDonald K, Running S, Frolking S (2004) Satellite radar remote sensing of seasonal growing seasons for boreal and subalpine evergreen forests. *Remote Sensing of Environment*, **90**, 243–258.

Kozlowski TT, Pallardy SG (1997) *Physiology of Woody Plants*. Academic Press, NY.

Kurz WA, Dymond C, Stinson G *et al*. (2008) Mountain pine beetle and forest carbon feedback to climate change. *Nature*, **452**, 987–990.

Legendre P (2010) Coefficient of concordance. In: *Encyclopedia of Research Design*, (ed. Salkind N), pp. 164–169. SAGE Publications, Inc., Los Angeles.

Linderholm H (2006) Growing season changes in the last century. *Agricultural and Forest Meteorology*, **137**, 1–14.

Liu YY, De Jeu RA, McCabe MF, Evans JP, Van Dijk AI (2011) Global long-term passive microwave satellite-based retrievals of vegetation optical depth. *Geophysical Research Letters*, **38**, L18402.

Los SO, Justice C, Tucker C (1994) A global 1 by 1 NDVI data set for climate studies derived from the GIMMS continental NDVI data. *International Journal of Remote Sensing*, **15**, 3493–3518.

Lucht W, Prentice I, Myneni R *et al*. (2002) Climatic control of the high-latitude vegetation greening trend and Pinatubo effect. *Science*, **296**, 1687.

Ma Z, Peng C, Zhu Q *et al*. (2012) Regional drought-induced reduction in the biomass carbon sink of Canada's boreal forests. *Proceedings of the National Academy of Sciences of the United States of America*, **109**, 2423–2427.

McDonald K, Kimball J, Njoku E, Zimmermann R, Zhao M (2004) Variability in springtime thaw in the terrestrial high latitudes: monitoring a major control on the biospheric assimilation of atmospheric CO_2 with spaceborne microwave remote sensing. *Earth Interactions*, **8**, 1–23.

Menzel A, Jakobi G, Ahas R, Scheifinger H, Estrella N (2003) Variations of the climatological growing season (1951–2000) in Germany compared with other countries. *International Journal of Climatology*, **23**, 793–812.

Menzel A, Sparks T, Estrella N *et al*. (2006) European phenological response to climate change matches the warming pattern. *Global Change Biology*, **12**, 1969–1976.

Myneni R, Keeling C, Tucker C, Asrar G, Nemani R (1997) Increased plant growth in the northern high latitudes from 1981 to 1991. *Nature*, **386**, 698–702.

Nemani R, Keeling C, Hashimoto H *et al*. (2003) Climate-driven increases in global terrestrial net primary production from 1982 to 1999. *Science*, **300**, 1560–1563.

Oksanen J, Blanchet F, Kindt R *et al*. (2011) *Vegan: Community Ecology Package. R Package Version 1.13-1*. Available at: http://vegan.r-forge.r-project.org. (accessed 27 August 2012).

Parmesan C, Yohe G (2003) A globally coherent fingerprint of climate change impacts across natural systems. *Nature*, **421**, 37–42.

Peng S, Chen A, Xu L *et al*. (2011) Recent change of vegetation growth trend in China. *Environmental Research Letters*, **6**, 044027.

Peñuelas J, Rutishauser T, Filella I (2009) Phenology feedbacks on climate change. *Science*, **324**, 887–888.

Piao S, Fang J, Zhou L, Ciais P, Zhu B (2006) Variations in satellite-derived phenology in China's temperate vegetation. *Global Change Biology*, **12**, 672–685.

Piao S, Friedlingstein P, Ciais P, Viovy N, Demarty J (2007) Growing season extension and its effects on terrestrial carbon flux over the last two decades. *Global Biogeochemical Cycles*, **21**, GB3018, doi: 10.1029/2006GB002888.

Piao S, Ciais P, Friedlingstein P *et al*. (2008) Net carbon dioxide losses of northern ecosystems in response to autumn warming. *Nature*, **451**, 49–52.

Piao S, Wang X, Ciais P, Zhu B, Wang T, Liu J (2011) Changes in satellite-derived vegetation growth trend in temperate and boreal Eurasia from 1982 to 2006. *Global Change Biology*, **17**, 3228–3239.

Randerson JT, Thompson MV, Conway TJ, Fung IY, Field CB (1997) The contribution of terrestrial sources and sinks to trends in the seasonal cycle of atmospheric carbon dioxide. *Global Biogeochemical Cycles*, **11**, 535–560.

Randerson JT, Field CB, Fung IY, Tans PP (1999) Increases in early season ecosystem uptake explain recent changes in the seasonal cycle of atmospheric CO_2 at high northern latitudes. *Geophysical Research Letters*, **26**, 2765–2768.

Raynolds MK, Walker DA, Epstein HE, Pinzon JE, Tucker CJ (2012) A new estimate of tundra-biome phytomass from trans-arctic field data and AVHRR NDVI. *Remote Sensing Letters*, **3**, 403–411.

Reed B, Brown J, VanderZee D, Loveland T, Merchant J, Ohlen D (1994) Measuring phenological variability from satellite imagery. *Journal of Vegetation Science*, **5**, 703–714.

Richardson A, Andy Black T, Ciais P *et al*. (2010) Influence of spring and autumn phenological transitions on forest ecosystem productivity. *Philosophical Transactions of the Royal Society B: Biological Sciences*, **365**, 3227.

Richardson AD, Keenan TF, Migliavacca M, Ryu Y, Sonnentag O, Toomey M (2013) Climate change, phenology, and phenological control of vegetation feedbacks to the climate system. *Agricultural and Forest Meteorology*, **169**, 156–173.

Robinson D, Dewey K, Heim R Jr (1993) Global snow cover monitoring: an update. *Bulletin of the American Meteorological Society*, **74**, 1689–1696.

Rosenthal SI, Camm EL (1997) Photosynthetic decline and pigment loss during autumn foliar senescence in western larch (Larix occidentalis). *Tree Physiology*, **17**, 767–775.

Sarmiento J, Gloor M, Gruber N *et al*. (2010) Trends and regional distributions of land and ocean carbon sinks. *Biogeosciences*, **7**, 2351–2367.

Schneider T (2001) Analysis of incomplete climate data: estimation of mean values and covariance matrices and imputation of missing values. *Journal of Climate*, **14**, 853–871.

Schwartz M, Ahas R, Aasa A (2006) Onset of spring starting earlier across the Northern Hemisphere. *Global Change Biology*, **12**, 343–351.

Smith N, Saatchi S, Randerson J (2004) Trends in high northern latitude soil freeze and thaw cycles from 1988 to 2002. *Journal of Geophysical Research*, **109**, D12101.

Soja AJ, Tchebakova NM, French NH *et al.* (2007) Climate-induced boreal forest change: predictions versus current observations. *Global and Planetary Change*, **56**, 274–296.

Stöckli R, Vidale P (2004) European plant phenology and climate as seen in a 20-year AVHRR land-surface parameter dataset. *International Journal Remote Sensing*, **25**, 3303–3330.

Suni T, Berninger F, Markkanen T, Keronen P, Rannik Ü, Vesala T (2003) Interannual variability and timing of growing-season CO_2 exchange in a boreal forest. *Journal of Geophysical Research*, **108**, 4265.

Tan B, Morisette J, Wolfe R, Gao F, Ederer G, Nightingale J, Pedelty J (2011) An enhanced TIMESAT algorithm for estimating vegetation phenology metrics from MODIS data. *IEEE Journal of Selected Topics in Applied Earth Observations and Remote Sensing*, **4**, 361–371.

Thoning K, Tans P, Komhyr W *et al.* (1989) Atmospheric carbon dioxide at Mauna Loa Observatory: 2, analysis of the NOAA GMCC data, 1974–1985. *Journal of Geophysical Research*, **94**, 8549–8565.

Trenberth KE, Jones PD, Ambenje P *et al.* (2007) Observations: surface and atmospheric climate change. In: *Climate Change 2007: The Physical Science Basis Contribution of Working Group I to the Fourth Assessment Report of the Intergovernmental Panel on Climate Change*, (eds Solomon S, Qin D, Manning M, Chen Z, Marquis M, Averyt KB, Tignor M, Miller HL), chap. 3, pp. 235–336. Cambridge University Press,Cambridge, UK.

Tucker C, Slayback D, Pinzon J, Los S, Myneni R, Taylor M (2001) Higher northern latitude normalized difference vegetation index and growing season trends from 1982 to 1999. *International Journal of Biometeorology*, **45**, 184–190.

Tucker C, Pinzón J, Brown M *et al.* (2005) An extended AVHRR 8-km NDVI dataset compatible with MODIS and SPOT vegetation NDVI data. *International Journal of Remote Sensing*, **26**, 4485–4498.

Vesala T, Launiainen S, Kolari P *et al.* (2010) Autumn temperature and carbon balance of a boreal scots pine forest in Southern Finland. *Biogeosciences*, **7**, 163–176.

Vitasse Y, Porté AJ, Kremer A, Michalet R, Delzon S (2009) Responses of canopy duration to temperature changes in four temperate tree species: relative contributions of spring and autumn leaf phenology. *Oecologia*, **161**, 187–198.

Wang X, Piao S, Ciais P, Li J, Friedlingstein P, Koven C, Chen A (2011) Spring temperature change and its implication in the change of vegetation growth in North America from 1982 to 2006. *Proceedings of the National Academy of Sciences of the United States of America*, **108**, 1240.

Warren JM, Norby RJ, Wullschleger SD (2011) Elevated CO_2 enhances leaf senescence during extreme drought in a temperate forest. *Tree Physiology*, **31**, 117–130.

Westerling AL, Hidalgo HG, Cayan DR, Swetnam TW (2006) Warming and earlier spring increase western US forest wildfire activity. *Science*, **313**, 940–943.

White M, Nemani R (2003) Canopy duration has little influence on annual carbon storage in the deciduous broad leaf forest. *Global Change Biology*, **9**, 967–972.

White M, De Beurs K, Didan K *et al.* (2009) Intercomparison, interpretation, and assessment of spring phenology in North America estimated from remote sensing for 1982–2006. *Global Change Biology*, **15**, 2335–2359.

Wu C, Gonsamo A, Chen JM *et al.* (2012) Interannual and spatial impacts of phenological transitions, growing season length, and spring and autumn temperatures on carbon sequestration: a North America flux data synthesis. *Global and Planetary Change*. **92–93**, 179–190.

Xu L, Myneni RB, Chapin FS III *et al.* (2013) Temperature and vegetation seasonality diminishment over northern lands. *Nature Climate Change*, **3**, 581–586. doi: 10.1038/nclimate1836.

Zeng H, Jia G, Epstein H (2011) Recent changes in phenology over the northern high latitudes detected from multi-satellite data. *Environmental Research Letters*, **6**, 045508.

Zhang K, Kimball J, Hogg E, Zhao M, Oechel W, Cassano J, Running S (2008) Satellite-based model detection of recent climate-driven changes in northern high-latitude vegetation productivity. *Journal of Geophysical Research*, **113**, G03–033.

Zhang K, Kimball J, Kim Y, McDonald K (2011) Changing freeze-thaw seasons in northern high latitudes and associated influences on evapotranspiration. *Hydrological Processes*, **25**, 4142–4151.

Zhang G, Zhang Y, Dong J, Xiao X (2013) Green-up dates in the Tibetan plateau have continuously advanced from 1982 to 2011. *Proceedings of the National Academy of Sciences of the United States of America*, **110**, 4309–4314.

Zhou L, Tucker C, Kaufmann R, Shabanov N, Myneni R (2001) Variations in northern vegetation activity inferred from satellite data of vegetation index during 1981 to 1999. *Journal of Geophysical Research*, **106**, 20–069.

Zhu W, Tian H, Xu X, Pan Y, Chen G, Lin W (2012) Extension of the growing season due to delayed autumn over mid and high latitudes in North America during 1982–2006. *Global Ecology and Biogeography*, **21**, 260–271.

Supporting Information

Additional Supporting Information may be found in the online version of this article:

Figure S1. Comparison of large-scale variations in the timing and length of the photosynthetic growing season showing that the results are not sensitive to the choice of the approach to extract phenology (see Methods section).
Figure S2. Comparison of variations in timing, length and intensity of the photosynthetic growing season between 1982 and 2006 based on the latest version of biweekly AVHRR NDVI data (GIMMS NDVI3g – green) and the earlier version of the dataset (GIMMS NDVIg – gray).
Figure S3. Comparison of variations in timing, length and intensity of the photosynthetic growing season between 2001 and 2011 based on 15-day AVHRR NDVI from the GIMMS NDVI3g data set (green) and on 16-day Terra MODIS NDVI from the MOD13C1 data set (gray).
Figure S4. Comparison of variations in the timing of spring snow melt based on NOAA weekly snow-cover (SMT – purple) with the timing of the SSM/I-based spring thaw (STH – black) and start of the thermal growing season (STS – orange) at latitudes north of 45°N.
Figure S5. Changes in spring and autumn number of non-frozen days based on satellite microwave (SSM/I – black) and gridded surface air temperature observations (HadGHCND – orange) north of 45°N. Correlations between the series for the period 1988-2007 and linear trends (β) for the HadGHCND series over the 1950-2011 period are given in each panel.
Figure S6. Comparison of 10-year high-pass filtered variations in seasonally integrated NDVI (green) with seasonally integrated temperature (orange), and peak-to-trough amplitude of the annual cycle of atmospheric CO_2 at Point Barrow (blue).
Figure S7. Comparison of parameters describing the amplitude and phase of the annual cycle of atmospheric CO_2 at northern latitudes based on observations at Point Barrow (71°N – blue) and on estimates from the marine boundary layer matrix of GLOBALVIEW–2011 averaged north of 60°N (red).
Figure S8. Correlation between growing season integrated GIMMS NDVI3g (TI–NDVI) and peak-to-trough amplitude of the annual cycle of atmospheric CO_2 at Point Barrow (black dot) from 1982 to 2010.

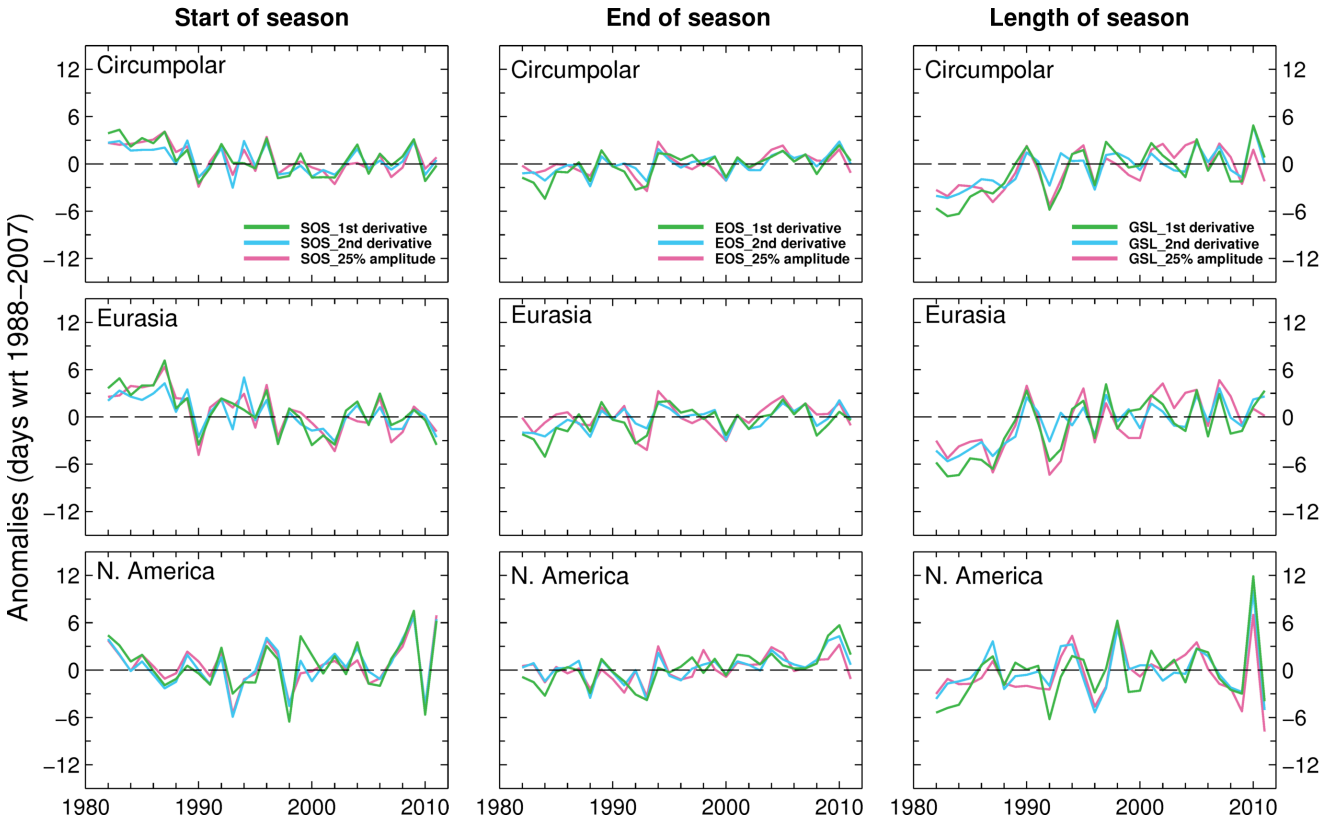

Supplemental Material, Figure S1: Comparison of large-scale variations of timing and length of the photosynthetic growing season showing that the results are not sensitive to variations in the method used to extract phenology (see *Methods section*). In this context, for a given 8-km grid box and year, the start of the photosynthetic growing season (SOS) corresponds to the time of the year when the NDVI rises above a threshold value in spring, while the end (EOS) occurs when the NDVI falls below a threshold value in autumn. In the first approach (*25% amplitude – pink*), an arbitrary threshold of 25% of the amplitude of the annual cycle of NDVI is used in spring and autumn each year. In the second approach (*1st derivative – green*), the spring and autumn NDVI thresholds used across all years in a given grid box correspond to the NDVI levels at which the inflection points for green-up and senescence occur in the first derivative of the 30-year NDVI climatology of that grid box. This is the method used to compute the phenological parameters presented in the manuscript. The third approach (*2nd derivative – cyan*) uses the NDVI levels for the inflection points for green-up and senescence in the second derivative of the 30-year NDVI climatology. Areas designated as water bodies, croplands, urban and barren or sparsely vegetated regions were masked out from analysis.

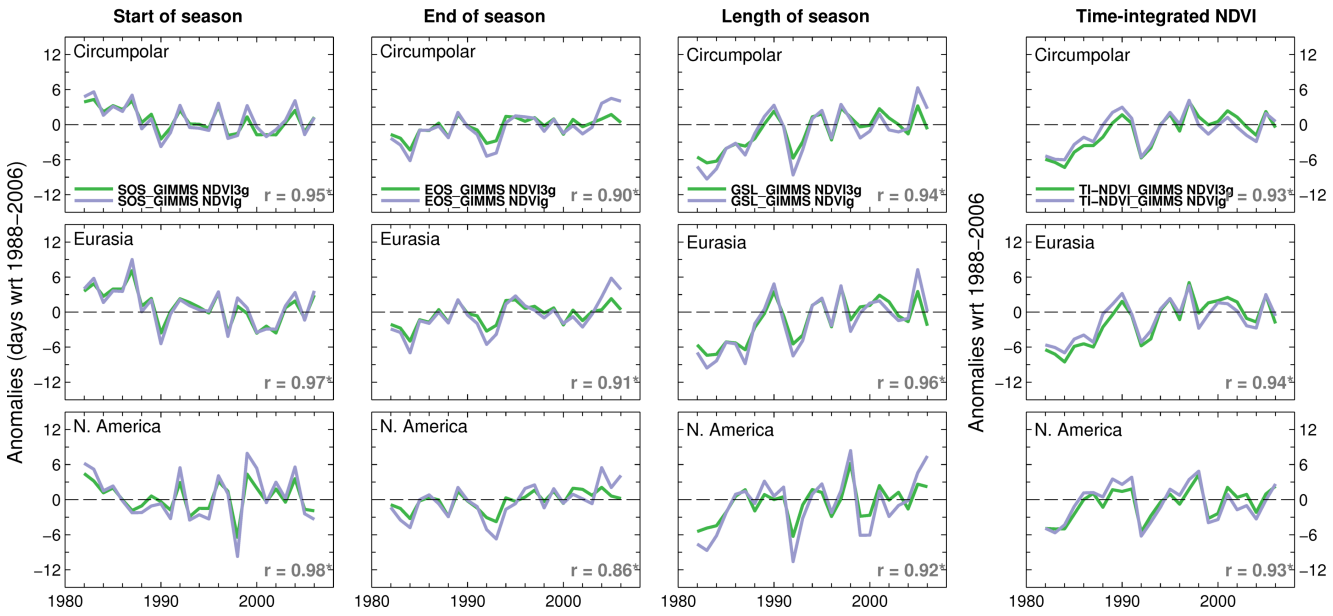

Supplemental Material, Figure S2: Comparison of variations in timing, length and intensity of the photosynthetic growing season between 1982 and 2006 based on the latest version of biweekly AVHRR GIMMS NDVI data (*GIMMS NDVI3g – green*) and the earlier version of the dataset (*GIMMS NDVIg – gray*). Inland water bodies, croplands, urban and barren or sparsely vegetated regions were excluded from the analysis.

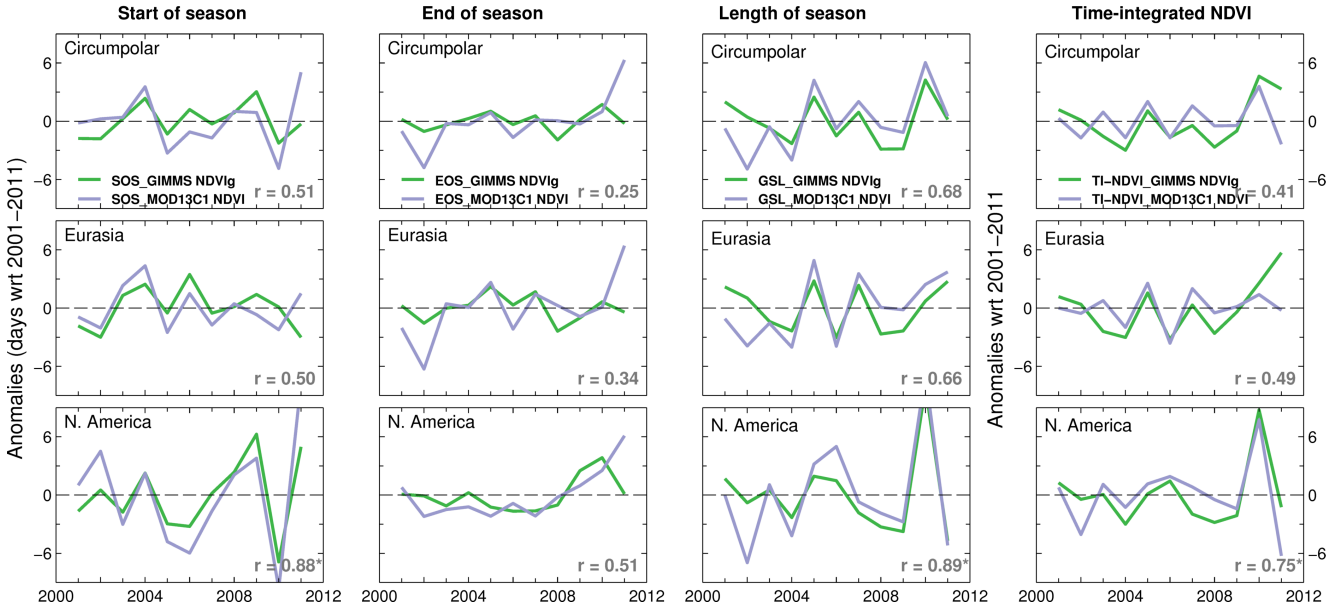

Supplemental Material, Figure S3: Comparison of variations in timing, length and intensity of the photosynthetic growing season between 2001 and 2011 based on 15-day AVHRR NDVI from the GIMMS NDVI3g dataset (*green*) and on 16-day Terra MODIS NDVI from the MOD13C1 dataset (*gray*). Inland water bodies, croplands, urban and barren or sparsely vegetated regions were excluded from the analysis.

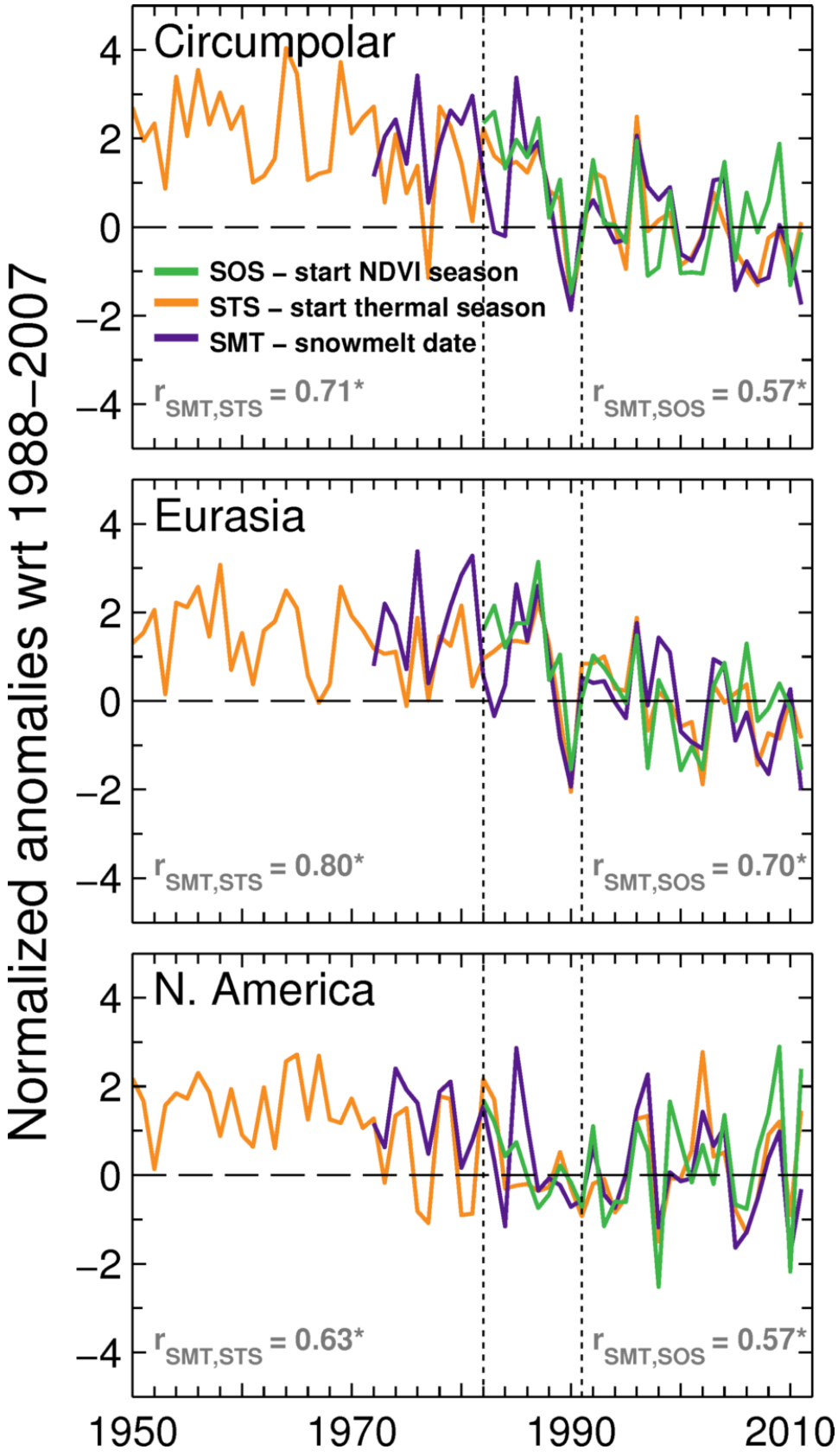

Supplemental Material, Figure S4: Comparison of variations in the timing of spring snowmelt based on NOAA weekly snow cover (*SMT – purple*) with the timing of start of the thermal growing season (*STS – orange*) and the start of the photosynthetic growing season (*SOS – green*) at latitudes north of 45°N. The correlations of SMT with STS and SOS over the common period 1982–2011 are shown in the lower-left and lower-right corner of each plot, respectively. An asterisk denotes significance at the $p < 0.05$ level. The vertical dotted lines indicate the eruptions of El Chichón in 1982 and Mount Pinatubo in 1991.

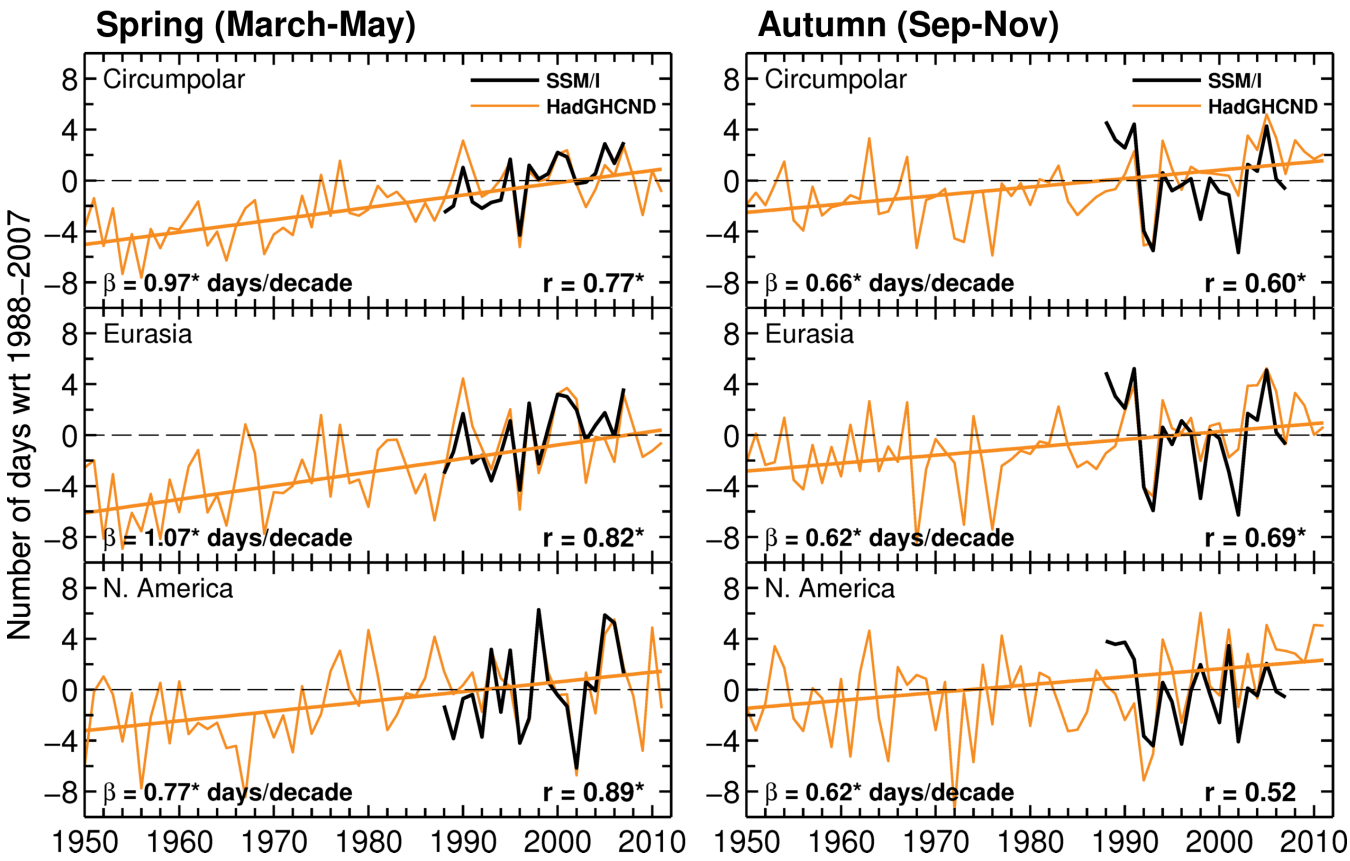

Supplemental Material, Figure S5: Changes in spring and autumn number of non-frozen days based on satellite microwave (*SSM/I – black*) and gridded surface air temperature observations (*HadGHCND – orange*) north of 45^{o}N. Correlations between the series for the period 1988-2007 and linear trends (β) for the HadGHCND series over the 1950-2011 period are given in each panel. An asterisk denotes significance at the $p < 0.05$ level.

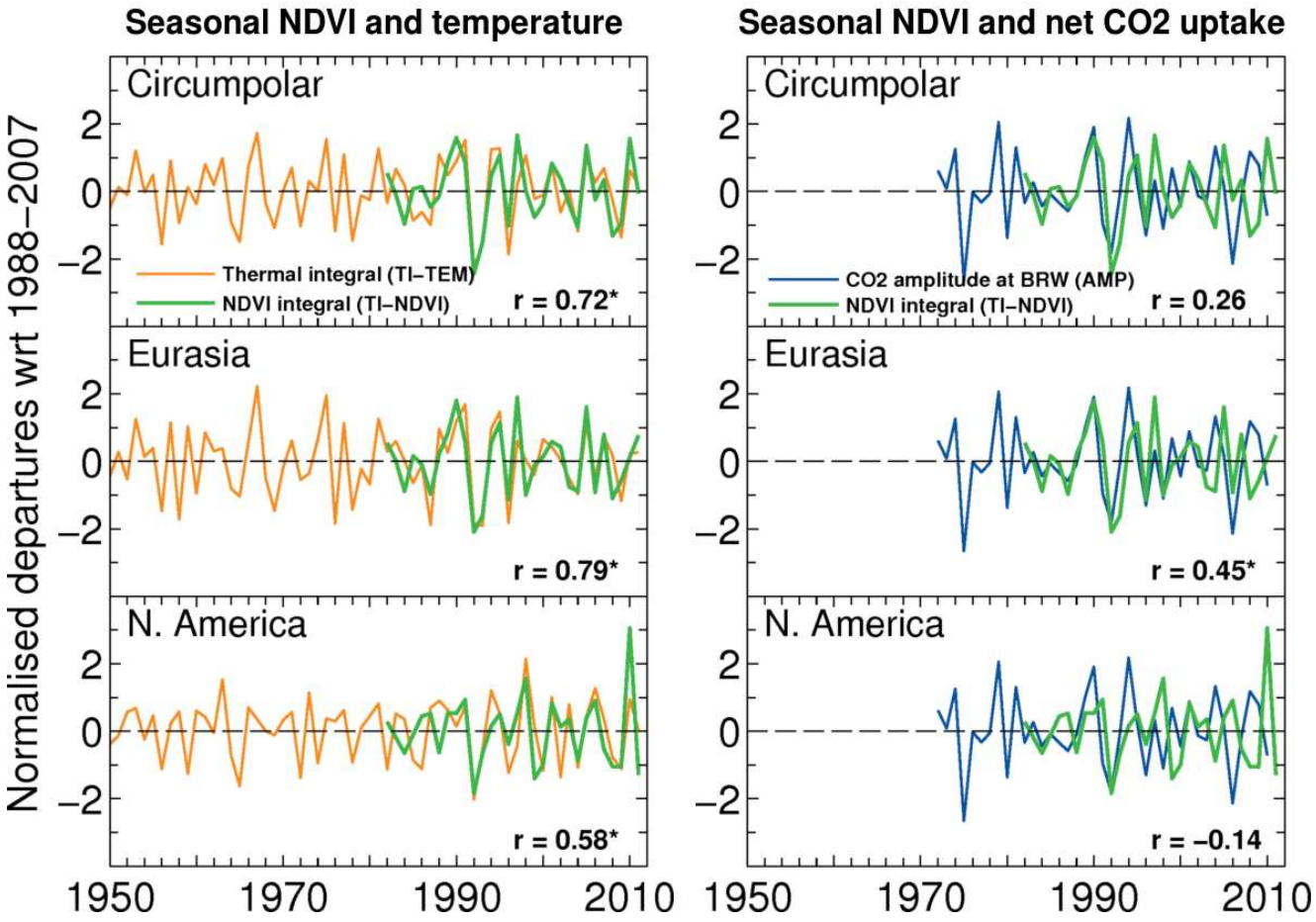

Supplemental Material, Figure S6: Comparison of 10-year high-pass filtered variations in seasonally integrated NDVI (*green*) with seasonally integrated temperature (*orange*), and peak-to-trough amplitude of the annual cycle of atmospheric CO_2 at Point Barrow (*blue*). The correlation between the series over their common period is shown in each panel. An asterisk denotes significance at the $p < 0.05$ level.

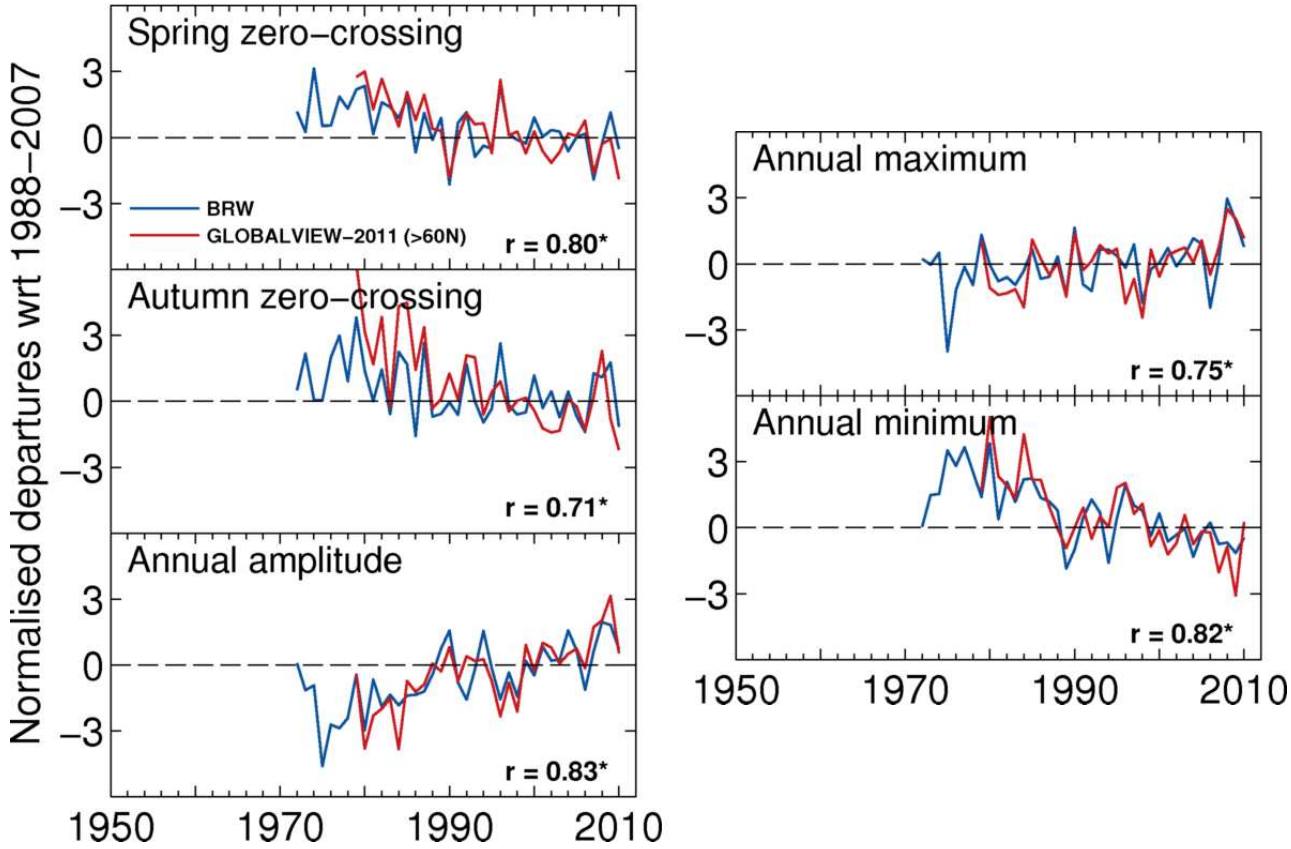

Supplemental Material, Figure S7: Comparison of changes in the amplitude and phase of the annual cycle of atmospheric CO_2 at northern latitudes based on observations at Point Barrow (*71°N – blue*) and on estimates from the marine boundary layer matrix of GLOBALVIEW–2011 averaged north of 60°N (*red*). The correlation between the series over the 1979–2010 period is shown in each panel. An asterisk denotes significance at the $p < 0.05$ level.

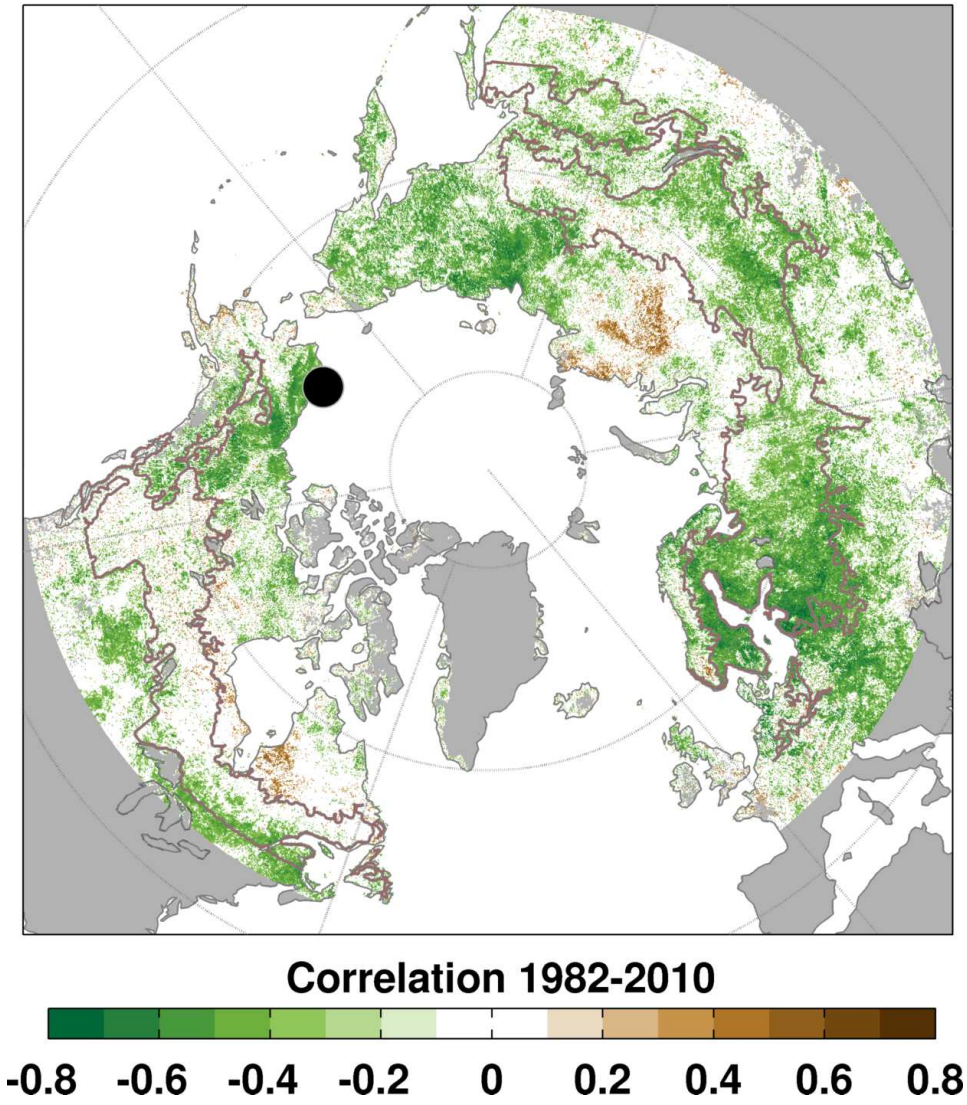

Supplemental Material, Figure S8: Correlation between growing season integrated GIMMS NDVI3g (TI–NDVI) and peak-to-trough amplitude of the annual cycle of atmospheric CO_2 at Point Barrow (*black dot*) from 1982 to 2010. Data were detrended prior to correlation analysis and only significant correlations ($p < 0.1$) are shown. The brown polygon indicates the extent of the needleleaf boreal forest.